Eur. Phys. J. Spec. Top. (2025) 234:3683–3703
https://doi.org/10.1140/epjs/s11734-024-01372-3

THE EUROPEAN PHYSICAL JOURNAL SPECIAL TOPICS

Regular Article

Event-triggered reachable set estimation for synchronization of Markovian jump complex-valued delayed neural networks under cyber-attacks

R. Vadivel[1,a], S. Sabarathinam[2,b], Guisheng Zhai[3,c], and Nallappan Gunasekaran[4,d]

[1] Department of Mathematics, Faculty of Science and Technology, Phuket Rajabhat University, Phuket 83000, Thailand
[2] Faculty of Computer Science, National Research University (HSE University), Moscow 109028, Russia
[3] Department of Mathematical Sciences, Shibaura Institute of Technology, Omiya, Saitama 337-8570, Japan
[4] Eastern Michigan Joint College of Engineering, Beibu Gulf University, Qinzhou 535011, China

Received 26 August 2024 / Accepted 10 October 2024 / Published online 28 October 2024

Abstract This paper focuses on the reachable set estimation for synchronizing of complex-valued neural networks (CVNNs) using an event-triggered (ET) approach and cyber-attacks. The system parameters are set up using Markovian switching rules. The proposed controller effectively saves the communication resources for the designed CVNNs. The main objective of this paper is to find an ellipsoid that can contain the state trajectory of the system as small as possible in the presence of control. From a physics point of view, the system can be likened to a dynamic system subjected to external perturbations, where the goal is to contain the trajectory of the system's state within a bounded region, similar to confining particle motion in phase space. To achieve this objective, we propose a novel approach based on the reachable set technique, which allows us to obtain an ellipsoid that contains the state trajectory of the system while minimizing its size. Utilizing the standard Lyapunov–Krasovskii functional (LKF), integral inequality approaches, some sufficient stability formed in terms of linear matrix inequalities (LMIs) are derived for the synchronization of CVNNs under the ET scheme, which can be solved using MATLAB's YALMIP toolbox. These conditions ensure that the states of the CVNNs converge to zero and that the synchronization error is bounded. Finally, numerical simulation results are provided to demonstrate the practicality and effectiveness of the proposed theoretical results.

1 Introduction

Since neurons join to form a typical complicated system, neural networks (NNs) have been extensively studied by academics and are applied in a wide range of fields, including machine learning, secure communication, and a variety of other domains. In addition, NNs have been the subject of increasing research attention during the past few decades [1, 2]. Integrating neural networks with physics has become a powerful approach to solving complex problems that require both data-driven models and physical insights. Physics-informed neural networks are designed to incorporate known physical laws (e.g., conservation of energy, momentum, thermodynamics, etc.) directly into the neural network's learning process. This hybrid approach improves the generalization and interpretability of the model while reducing the need for large amounts of training data [3, 4]. Neural networks are increasingly being used to model chaotic systems. These are systems that are highly sensitive to initial conditions, like weather patterns or fluid turbulence [5]. Complex networks such as those describing interactions in materials (e.g., lattice networks, spin systems) or biological systems can be analyzed using graph neural networks (GNNs) [6]. These networks learn from the topological structure of the data, providing insights into the emergent properties of the system such as phase transitions, synchronization in complex systems, and network-based diffusion phenomena.

[a] e-mail: vadivelsr@yahoo.com
[b] e-mail: saba.cnld@gmail.com
[c] e-mail: zhai@shibaura-it.ac.jp (corresponding author)
[d] e-mail: gunasmaths@gmail.com (corresponding author)

Neural networks are used for optimization in various areas of physics such as material science [7], modeling physical phenomena [8], quantum neural networks [9], etc. The authors have suggested using complex-valued fields to show states, connection weights, and activation functions in neural networks (NNs). These are called complex-valued neural networks (CVNNs) [10, 11]. If you want to simplify the model structure, improve learning, and shorten training time, CVNNs are better than real-valued neural networks (RVNNs) [12, 13]. Also, CVNNs might be able to solve problems that RVNNs cannot, such as the exclusion OR (XOR) and the finding of symmetry [14, 15]. It demonstrates that CVNNs have superior computational capabilities and execution. As a result, CVNNs have received increasing attention recently. Meanwhile, since neurons can only send and process signals at a certain rate, temporal delays will always occur in actual CVNN implementations. These delays frequently manifest as discretization and distribution [16, 17]. It is well known that time delays may significantly affect how dynamically a system performs and potentially induce several instability characteristics. Several works on the dynamics analysis and control synthesis of CVNNs with various time delays have been published recently.

In a different field of study, Markov jumps are often used to make models where parameters and structures change quickly and randomly due to noise in the environment, broken actuators, and other things. Markov jumping (MJ) systems specifically perform well with a wide range of real-time applications, including wireless communication networks, nuclear power plants, and the management of aircraft [18–20]. The class of stochastic finite subsystems that the Markov chain governs makes up the jumping systems. Studies of NNs with Markovian jumping parameters have drawn a lot of attention from researchers because of their distinctive modeling capacity. Some important findings about the dynamic behavior of Markovian jumping systems are presented in [21, 22]. For example, [23] investigated the exponential stability of CVNNs with the MJS approach. At the same time, the concept of finite/fixed time synchronization was proposed for CV memristive NNs [22]. Recently, [21] studied the stochastic stability of fractional-order MJ CVNNs. However, the combination of MJ with CVNNS for system performance analysis is also challenging and interesting.

Synchronization has received a lot of attention because it is a common and important group behavior of NNs. Synchronization of CVNNs can help in harmonic oscillation synthesis, secure connectivity, information science, and other fields related to engineering [16, 24–27]. As a result, it is worthwhile investigating the synchronization behavior of CVNNs. In their pioneering work, Pecora and Carroll (1990) developed the notion of master–slave synchronization for the first time [28]. Furthermore, synchronization of master–slave systems has become a popular study issue, particularly for CVNNs. Several studies addressing the master–slave synchronization problem of NNs have been suggested in recent years [29–32]. Guo et al. [16] proposed quasiprojective synchronization for delayed stochastic CVNNS. Yuan et al. [29] concentrated on CVNNS with mixed two additive time-varying delays, which were considered for the synchronization error system. Recently, [33] used event-triggered synchronization to study stochastic delayed neural networks in the cases of passivity and passification. Moreover, in control theory, the estimate of reachable sets is now a hot issue. The task is to make an ellipsoid that contains all the state paths that the system being studied takes with limited input and a starting point of zero [34, 35]. The Lyapunov function approach has made significant advances in recent decades for the estimate of reachable sets (RSE) [36, 37]. As master–slave NN synchronization cannot be accomplished without external control, it is crucial to build efficient controllers to include in the slave system to establish controlled synchronization with the master system.

On the other hand, if the network as a whole has limited capacity or slow transmission speeds, it might be difficult to reach each node individually. As a result, the performance of the network will suffer since data transmission across all networks consumes a greater portion of available capacity [26, 33, 38, 39]. Although few attempts to provide synchronization control for CVNNs using a reachable set estimation architecture have been successful, making the most efficient use of the limited communication bandwidth has emerged as a critical concern. To examine the problem mentioned above, the event-triggered mechanism (ET) has been developed as a promising approach to conserve limited network resources [26, 26, 27, 40]. Furthermore, the network system is frequently attacked in operation because of its open nature and the uncertainty of the network environment. As a result, protecting the network infrastructure has emerged as a vital area of study in the field of control systems. Some of the greatest studies on network security challenges have been proposed to defend against cyber-attacks and make perfect attacks impossible [41, 42]. For example, [43] investigated event-triggered synchronization control for complex networks with quantization and cyber-attacks. Event-triggered exponential synchronization was addressed for complex-valued memristive neural networks [26]. Moreover, [27] concerns the issue of event-based master–slave synchronization of complex-valued neural networks through an impulsive control. To our knowledge, there are few results on the synchronization of event-triggered CVNNS research on reachable set estimation and cyber-attacks that deserve more attention, which is the second motivation that led to our current study.

Based on the aforementioned discussions, this paper focuses on the event-triggered reachable set estimation for the synchronization of CVNNS under cyberattacks. The Lyapunov–Krasovskii functional method and the linear matrix inequality approach are employed to present adequate conditions that ensure synchronization. The novelty of this article is listed below.

(i) Compared to the existing literature, in this work, an event-triggered mechanism with cyberattack is adopted in the complex domain to improve the efficiency of data transmission, which can significantly decrease the communication frequency between nodes and save network resources when addressing CVNN synchronization.
(ii) By utilizing novel inequality techniques, some sufficient conditions are presented by employing the appropriate Lyapunov–Krasovskii functional (LKF) method and Linear Matrix Inequality (LMI) technique, which can ensure the synchronization of the complex network can be the reachable set to be bound by the intersection of ellipsoids and can be solved by YALMIP toolbox in MATLAB.
(iii) Finally, a numerical example is presented to illustrate the correctness of the derived result in this paper.

Notations: $\mathbb{C}^n$ and $\mathbb{C}^{n\times m}$ denote, respectively, the set of all n-dimensional complex-valued vectors and the set of all $n \times m$ complex-valued matrices. In that order, the notation $Re(Y)$, $Im(Y)$, and Y^* represent the real, imaginary, and conjugate transpose of matrix Y. I stands for the identity matrix with the required dimension. ★ designates the transposed element in symmetrical locations; $X > Y (X < Y)$ denotes a positive (negative) definite matrix for $X - Y$, while $X \geq Y (X \leq Y)$ denotes a positive (negative) semidefinite matrix for $X - Y$. In addition, the definition of $\mathrm{Sym}\{X\}$ is $X + X^*$. The block-diagonal matrix is denoted by $\mathrm{diag}\{...\}$. $col\{x^1, x^2, ..., x^n\}$ means $[x^{1*}, x^{2*}, ..., x^{n*}]^*$. The spectral norm for matrices and the Euclidean norm for vector space is denoted by the symbol $||\cdot||$. Moreover, let $\{e_t, t \geq 0\}$ be a right continuous Markov process on the probability space which takes values in the finite set $\mathcal{N} = \{1, 2, ..., n\}$ with transition probability matrix $\Pi \triangleq \{\pi_{\rho j}\}$ given by

$$\mathbb{P}\{e_{t+\Delta t} = j | e_t = \rho\} = \begin{cases} \pi_{\rho j}\Delta + o(\Delta t), & \rho \neq j \\ 1 + \pi_{\rho j}\Delta t + o(\Delta t), & \rho = j \end{cases}$$

where $\Delta t > 0$, $\lim_{\Delta t \to 0} \frac{o(\Delta t)}{\Delta t} = 0$ and $\pi_{\rho j} \geq 0$ is the transition rate from ρ to j, if $\rho \neq j$ and $\pi_{\rho\rho} = -\sum_{j=1, j\neq\rho}^{n} \pi_{\rho j}$.

2 Mathematical preliminaries

This paper considers a class of master ($\mathscr{M}$) slave ($\mathscr{S}$) synchronization of delayed CVNNs described by:

$$\begin{cases} \dot{y}(t) &= -\bar{M}_{e_t} y(t) + \bar{N}_{e_t} g(y(t)) + \bar{O}_{e_t} g(y(t - \partial(t))), \\ \dot{z}(t) &= -\bar{M}_{e_t} z(t) + \bar{N}_{e_t} g(z(t)) + \bar{O}_{e_t} g(z(t - \partial(t))) + u(t) + E_{e_t} w(t). \end{cases} \tag{1}$$

Here, $y(\cdot) \in \mathbb{C}^n$ represents the state vector; $g(y(\cdot))$ and $g(z(\cdot)) \in \mathbb{C}^n$ are stated as the neuron activation function with complex values. $\bar{M}_{e_t}$ denotes the positive diagonal matrix; $\bar{N}_{e_t}$ and $\bar{O}_{e_t}$ represent the connection weight and the delayed connection weight matrices; E_{e_t} are referred to as constant matrices; the control input is indicated as $u(t)$; $w(t)$ is noted as disturbance, which satisfies $w^T(t)w(t) \leq \hat{w}^2$, where $\hat{w}$ is constant. The time delay $\partial(t)$ satisfies

$$0 \leq \partial(t) \leq \partial_1, \ \ \dot{\partial}(t) \leq \mu, \tag{2}$$

where ∂_1 and μ are positive constants.

Assumption 1 The activation function $g_i(\cdot)$ in g is continuous, that is, there exist constants $\hat{X}_s^-$ and $\hat{X}_s^+$, holds

$$\hat{X}_s^- \leq \frac{g_s(k_1) - g_s(k_2)}{k_1 - k_2} \leq \hat{X}_s^+,$$

where $k_1, k_2 \in \mathbb{C}$ and $k_1 \neq k_2$, $s = 1, 2, ..., n$.

From (1) with $r(t) = z(t) - y(t)$, the error system is obtained as

$$\begin{aligned} \dot{r}(t) = &-\bar{M}_{e_t} r(t) + \bar{N}_{e_t} f(r(t)) + \bar{O}_{e_t} f(r(t - \partial(t))) \\ &+ u(t) + E_{e_t} w(t), \end{aligned} \tag{3}$$

where $f(r(t)) = g(z(t)) - g(y(t))$. Also, the function $f_s(\cdot)$ satisfies the following requirement:

$$\hat{X}_s^- \leq \frac{f_s(r)}{r} \leq \hat{X}_s^+, \ \ s = 1, 2, ..., n, \tag{4}$$

where $r \in \mathbb{C}$ and $r \neq 0$.

Throughout this study, we will accept that the modeled framework (3) is monitored by a network organization. The sensors use the ET sampler technique, which means that the defined signal only reformulates its output to fulfill the ET specification. This ET specification is for the sampled-data $\{r(i\tau) \mid i \in N\}$, where τ is a fixed sampling interval. When the current sampled-data $r((k+i)\tau)$ and the latest communication $r(k\tau)$ satisfy the following event condition:

$$[r((k+i)\tau) - r(k\tau)]^T \Theta_{e_t} [r((k+i)\tau) - r(k\tau)] \quad \geq \phi r^T(k\tau) \Theta_{e_t} r(k\tau),\ i \in N_+ \tag{5}$$

Θ_{e_t} denotes a Hermitian matrix, and ϕ is contained in the interval [0,1). Based on (5), $t_0\tau$, $t_1\tau$, $t_2\tau$, ..., represents the release times with $t_0 = 0$ as the beginning point. In this case, the time range for release within the sampling duration specified in (5) is indicated by $\nu_j\tau = t_{j+1}\tau - t_j\tau$. We used the following state-feedback technique to measure network-induced delay (NID).

$$u(t) = K_\rho r(t),\ t \in [t_k\tau + \eta_k,\ t_{k+1}\tau + \eta_{k+1}). \tag{6}$$

The NID is denoted by $\eta_k \in [0, \eta)$, η is a positive real number, and K_{e_t} are the controller gains to be designed later. The following process then transforms the error system given in (3) into a time-delay model. First, we partition the time interval $[t_k\tau + \eta_{t_k},\ t_{k+1}\tau + \eta_{t_{k+1}})$ into $t_{k+1} - t_k$ sub-intervals.

$$[t_k\tau + \eta_k,\ t_{k+1}\tau + \eta_{k+1}) \quad = \bigcup_{m=0}^{s} [t_k\tau + m\tau + \eta,\ t_k\tau + (m+1)\tau + \eta). \tag{7}$$

Moreover, with the definition of $\eta(t)$ and $e(t)$ in [44], we propose a novel controller design approach that incorporates an event-triggered scheme and takes into account the possibility of cyber-attacks

$$u(t) = \beta(t_k) K_{e_t} [r(t - \eta(t)) + \tilde{e}(t)] \quad + (1 - \beta(t_k)) K_{e_t} g(r(t - d(t))), \tag{8}$$

where $\beta(t_k) \in \{0, 1\}$ with the following statistical properties: $Prob\{\beta(t_k) = 1\} = \bar{\beta}$, $Prob\{\beta(t_k) = 0\} = 1 - \bar{\beta}$, K_{e_t} is the control gain matrix, which is determined later, $g(r(t - d(t)))$ is the function of cyber-attacks, $g(r(t)) \in \mathbb{C}^n$, $d(t) \in (0,\ d_2]$, d_2 is a positive constant. Substituting (8) into (3), we have

$$\begin{aligned} \dot{r}(t) = &-\bar{M}_{e_t} r(t) + \bar{N}_{e_t} f(r(t)) + \bar{O}_{e_t} f(r(t - \partial(t))) + \beta(t_k) K_{e_t} [r(t - \eta(t)) + \tilde{e}(t)] \\ &+ (1 - \beta(t_k)) K_{e_t} \times g(r(t - d(t))) + E_{e_t} w(t), \end{aligned} \tag{9}$$

where $t \in [t_k\tau + \eta_k,\ t_{k+1}\tau + \eta_{k+1})$. Recalling the definition of $\eta(t)$ and the characteristics of $\beta(t_k)$, (9) can be obtained as

$$\begin{aligned} \dot{r}(t) = &-\bar{M}_{e_t} r(t) + \bar{N}_{e_t} f(r(t)) + \bar{O}_{e_t} f(r(t - \partial(t))) \quad + \bar{\beta} K_{e_t} [r(t - \eta(t)) + \tilde{e}(t)] \\ &+ (1 - \bar{\beta}) K_{e_t} \times g(r(t - d(t))) + E_{e_t} w(t) \quad + (\beta(t_k) - \bar{\beta}) K_{e_t} [r(t - \eta(t)) \\ &+ \tilde{e}(t) - g(r(t - d(t)))],\ \ t \in [t_k\tau + \eta_k,\ t_{k+1}\eta + \eta_{k+1}). \end{aligned}$$

For convenience, setting $\bar{M}_{e_t} = \bar{M}_\rho$, $\bar{N}_{e_t} = \bar{N}_\rho$, $\bar{O}_{e_t} = \bar{O}_\rho$, $E_{e_t} = E_\rho$, $K_{e_t} = K_\rho$. Therefore, we have

$$\begin{aligned} \dot{r}(t) = &-\bar{M}_\rho r(t) + \bar{N}_\rho f(r(t)) \quad + \bar{O}_\rho f(r(t - \partial(t))) + \bar{\beta} K_\rho [r(t - \eta(t)) + \tilde{e}(t)] \\ &+ (1 - \bar{\beta}) K_\rho g(r(t - d(t))) + E_\rho w(t) \quad + (\beta(t_k) - \bar{\beta}) K_\rho [r(t - \eta(t)) \\ &+ \tilde{e}(t) - g(r(t - d(t)))],\ \ t \in [t_k\tau + \eta_k,\ t_{k+1}\eta + \eta_{k+1}). \end{aligned} \tag{10}$$

Based on the [45] For $\forall t \geq 0$, the error system (10) is outlined as:

$$\mathscr{R}_x = \{r(t) \mid r(t) \text{ and } w(t) \text{ satisfy } w^*(t) w(t) \leq \hat{w}^2,\ \ t \geq 0\}, \tag{11}$$

and an ellipsoid is employed to enclose the reachable set of error system (10) and defining $\epsilon(P) = \{\xi \mid \xi^* P \xi \leq 1,\ \xi \in \mathbb{C}^n,\ P > 0\}$.

Remark 1 With the description of $\eta(t)$, we have $0 \leq \eta(t) \leq \tau + h$, $\dot{\eta}(t) = 1$ and note $\eta_1 = \tau + h$. Therefore, we have $0 \leq \eta(t) \leq h_2$. Moreover, from (5) and the definition of $\tilde{e}(t)$, yields

$$\tilde{e}^*(t)\Theta_{e_t}\tilde{e}(t) \leq \phi r^*(t - \eta(t))\Theta_{e_t} r(t - \eta(t)). \tag{12}$$

Assumption 2 [46] The cyber-attack function $g_i(r)$ satisfies $g_i(0) = 0$ and $\forall i \in \{1, 2, ..., n\}$, $n_1 \neq n_2$

$$\bar{\phi}_{gi}^{-} \leq \frac{g_i(n_1) - g_i(n_2)}{n_1 - n_2} \leq \bar{\phi}_{gi}^{+},$$

where $\bar{\phi}_{gi}^{-}$ and $\bar{\phi}_{gi}^{+}$ are known constants.

The primary results are derived from the upcoming lemmas.

Lemma 1 [45] Let $V(x(t))$ be a differentiable Lyapunov function for the system (10) with $V(x(0)) = 0$ and $\hat{w}(t)$ satisfying (2). Also, for $a > 0$ and defining $\dot{V}(x(t)) + aV(x(t)) - \frac{a}{w_m} w^*(t)w(t) \leq 0$ we have $V(x(t)) \leq 1$.

Lemma 2 [47] For every Hermitian matrix $R > 0$, given integer S, any vector ξ, any continuously differentiable function $x : [-\tau, 0] \to \mathbb{C}^n$, and slack matrices M, N, it holds.

$$\begin{aligned}
-\tau \int_{t-\tau}^{t} \dot{x}^*(s)R\dot{x}(s)ds \leq\ & \xi^*(t)[\tau(t)M^*\hat{R}^{-1}M + h_\tau N^*\hat{R}^{-1}N] \\
& + \left(\frac{h_\tau}{\tau} + \frac{\tau(t)^2}{\tau^2}\right) Sym[\nu^*(t - \tau(t), t)\Gamma_a^* M \\
& + \nu^*(t - \tau, t - \tau(t))\Gamma_a^* N]\xi \\
& - \left\{ \frac{h_\tau}{\tau}\nu^*(t - \tau(t), t)\Gamma_a^* M\hat{R}\Gamma_a \nu(t - \tau(t), t) \right. \\
& \left. + \frac{\tau(t)^2}{\tau^2}\nu^*(t - \tau, t - \tau(t))\Gamma_a^* M\hat{R}\Gamma_a(t - \tau, t - \tau(t)) \right\},
\end{aligned}$$

where

$$\begin{aligned}
\hat{R} &= diag\{R, 3R, ..., (2S + 1)R\}, \\
\Gamma_a &= col[\pi_s(0), \pi_s(1), ..., \pi_s(S)], \\
\xi(t) &= col[x(t), x(t - \tau(t)), x(t - \tau), \dot{x}(t - \tau(t)), \dot{x}(t - \tau), \omega_1(t - \tau(t), t), \\
&\quad \omega_1(t - \tau, t - \tau(t)), \omega_2(t - \tau(t), t), \omega_2(t - \tau, t - \tau(t))], \\
\omega_1(a, b) &= \frac{1}{(b - a)} \int_a^b x(s)\mathrm{d}s, \\
\omega_1(a, b) &= \frac{1}{(b - a)^2} \int_a^b \int_u^b x(s)dsdu.
\end{aligned}$$

and other terms are defined in Lemma 1 of [47].

Lemma 3 [48] Given $\mathscr{W} \in \mathbb{C}^{n\times n} > 0$, a vector $Y : [a_1, a_2] \to \mathbb{C}^n$, and an auxiliary scalar function $\{k_i(l) | l \in [a_1, a_2], k_0(l) = 1\}$ satisfying $\int_{a_1}^{a_2} k_i(\theta)k_l(\theta)\mathrm{d}s = 0$, $(0 \leq i, l \leq n, i \neq l)$ with $k_i(\theta)(i = 1, ..., n)$ not identically zero. For any matrices $M_i \in \mathbb{C}^{k\times n}(i = 0, ..., n)$ and a vector $\tau \in \mathbb{C}^k$ the following inequality satisfies:

$$-\int_{a_1}^{a_2} Y^*(\theta)\mathscr{W}Y(\theta)d\theta \leq \tau^* \left\{ \sum_{i=0}^{n} \int_{a_1}^{a_2} k_i^2(\theta)d\theta \quad \times M_i\mathscr{W}^{-1}M_i^* + \mathrm{sym}\left(\sum_{i=0}^{n} M_i\alpha_i\right) \right\}\tau, \tag{13}$$

where $\alpha_i \in \mathbb{R}^{n\times k}(i = 0, ..., n)$, and $\int_{a_1}^{a_2} k_i(\theta)Y(\theta)d\theta = \alpha_i\tau$.

Lemma 4 [49] For any Hermitian matrix $H_{33} > 0$, and arbitrary matrices H_{11}, H_{12}, H_{13}, H_{22} and H_{23} such that $H = \begin{bmatrix} H_{11} & H_{12} & H_{13} \\ \star & H_{22} & H_{23} \\ \star & \star & H_{33} \end{bmatrix} \geq 0$, then we obtain

$$-\int_{t-\eta(t)}^{t} \dot{r}^*(s) H_{33} r(s) \mathrm{d}s \leq -\int_{t-\eta(t)}^{t} \begin{bmatrix} r(t) \\ r(t-\eta(t)) \\ \dot{r}(s) \end{bmatrix}^* \begin{bmatrix} H_{11} & H_{12} & H_{13} \\ \star & H_{22} & H_{23} \\ \star & \star & 0 \end{bmatrix} \begin{bmatrix} r(t) \\ r(t-\eta(t)) \\ \dot{r}(s) \end{bmatrix} \mathrm{d}s.$$

3 Main results

We will provide some sufficient conditions in subsequent theorems to achieve the bounding of reachable set of the suggested CVNNs using the ET technique while cyber-attacks are present. For simplicity, set

$$\begin{aligned}
\jmath_l &= [0_{n\times(l-1)}\ I_n\ 0_{n\times(17-l)n}]^*, \\
l &= 1, 2, ..., 17,\ \ \hat{J}_i = \tilde{e}_i \mathscr{S}_i,\ (i = 1, 2), \\
\tilde{e}_i &= [r(t)\ r(t-\partial(t))\ r(t-\partial_1)\ m_1(t)\ m_2(t)\ m_3(t)\ m_4(t)], \\
\partial_{1t} &= (\partial_1 - \partial(t)) \\
\hat{\varsigma}_1 &= col[\jmath_1 - \jmath_2,\ \jmath_1 + \jmath_2 - 2\jmath_6,\ \jmath_1 + \jmath_2 + 6\jmath_6 - 12\jmath_8], \\
\hat{\varsigma}_2 &= col[\jmath_2 - \jmath_3,\ \jmath_2 + \jmath_3 - 2\jmath_7,\ \jmath_2 + \jmath_3 + 6\jmath_7 - 12\jmath_9], \\
\Omega_1 &= [\partial(t)m_1(t)\ \ r(t) - r(t-\partial(t))\partial_{1t}m_2(t)r(t-\partial(t)) - r(t-\partial_1)], \\
\Omega_2 &= [\partial(t)(-m_1(t) + 2m_3(t))r(t) + r(t-\partial(t)) - 2m_1(t)\partial_{1t}(-m_2(t) + 2m_4(t))r(t-\partial(t)) + r(t-\partial_1) - 2m_2(t)], \\
\chi^*(t) &= [r^*(t)\ r^*(t-\partial(t))\ r^*(t-\partial_1)\ f^*(r(t))f^*(r(t-\partial(t)))\ m_1^*(t)\ m_2^*(t)\ m_3^*(t)\ m_4^*(t) \\
&\quad \dot{r}^*(t)\ r^*(t-\eta(t))\ r^*(t-h_2)\ \tilde{e}^*(t)\ r^*(t-d(t))r^*(t-d_2)\ g^*(r(t-d(t)))\ w^*(t)], \\
\mho^*(t) &= [\jmath_1^*(t)\ \jmath_{10}^*(t)],\ \ \tilde{\mathscr{G}}_n = diag\{\hat{\mathscr{G}}_n,\ 3\hat{\mathscr{G}}_n\}, \\
m_1(t) &= \int_{t-\partial(t)}^{t} \frac{r(s)}{\partial(t)} \mathrm{d}s, \\
m_2(t) &= \frac{1}{\partial_{1t}} \int_{t-\partial_1}^{t-\partial(t)} r(s) \mathrm{d}s, \\
m_3(t) &= \frac{1}{(\partial(t))^2} \int_{t-\partial(t)}^{t} \int_{\theta}^{t} r(u) du d\theta,\ \tilde{\mathscr{G}}_m = diag\{\hat{\mathscr{G}}_m,\ 3\hat{\mathscr{G}}_m\}, \\
m_4(t) &= \frac{1}{(\partial_{1t})^2} \int_{t-\partial_1}^{t-\partial(t)} \int_{\theta}^{t-\partial(t)} r(u) du d\theta, \\
\Theta_{01}(\partial(t)) &= \left(\frac{\partial_{1t}}{\partial_1} + \frac{(\partial(t))^2}{\partial_1^2}\right) sym[\hat{Y}_1^* \hat{\varsigma}_1 + \hat{Y}_2^* \hat{\varsigma}_2] \quad - \left(\frac{\partial_{1t}}{\partial_1^2} \hat{\varsigma}_1^* \mathscr{G}_2 \hat{\varsigma}_1 + \frac{\partial(t)}{\partial_1^2} \hat{\varsigma}_2^* \mathscr{G}_2 \hat{\varsigma}_2\right), \\
\hat{\Theta}_{01}(\partial(t)) &= \partial(t) \hat{Y}_1^* \mathscr{G}_2^{-1} \hat{Y}_1 + (\partial_1 - \partial(t)) \hat{Y}_2^* \mathscr{G}_2^{-1} \hat{Y}_2.
\end{aligned}$$

Theorem 1 For given positive scalars, ∂_1, μ, h_2, ϕ, d_2, $\alpha > 0$, and gain matrices K_ρ, if there exist Hermitian matrices $P_\rho > 0$, $J_s > 0 (s = 1, 2, 3)$, $\mathscr{G}_1 \in \mathbb{C}^{2n\times 2n} > 0$, $\mathscr{G}_i > 0 (i = 2, 3, 4)$, $\mathscr{G}_m > 0$, $\mathscr{G}_n > 0$, $\mathscr{K}_1 > 0$, positive diagonal matrices $\hat{\Lambda}_r > 0 (r = 1, 2)$, $\mathcal{V}$, and appropriate dimensional matrices $\mathscr{S}_i \in \mathbb{C}^{7n\times 4n}$, $(i = 1, 2)$, $\hat{Y}_1$, $\hat{Y}_2$, $\mathscr{W}_l (l = 1, 2, 3, 4)$, $\Theta_\rho > 0$, such that

$$\begin{bmatrix} \mathscr{G}_4 & \mathscr{K}_1 \\ \star & \mathscr{G}_4 \end{bmatrix} \geq 0 \tag{14}$$

$$\begin{bmatrix} \tilde{\Psi}_{[\partial(t)=0]} & \tilde{\Psi}_{12} & \tilde{\Psi}_{13} \\ \star & \tilde{\Psi}_{22} & 0 \\ \star & \star & \tilde{\Psi}_{33} \end{bmatrix} < 0 \tag{15}$$

$$\begin{bmatrix} \tilde{\Psi}_{[\partial(t)=\partial_1]} & \bar{\Psi}_{12} & \bar{\Psi}_{13} \\ \star & \bar{\Psi}_{22} & 0 \\ \star & \star & \bar{\Psi}_{33} \end{bmatrix} < 0 \tag{16}$$

where

$$\tilde{\Psi}_{[\partial(t)]} = \sum_{i=1}^{7} \Xi_i + \tilde{\Xi}_{11},$$

$$\Xi_1 = \jmath_1 P_\rho \jmath_{10} + \jmath_1 \alpha P_\rho \jmath_1 + \jmath_1^* \sum_{j=1}^{N} \Pi_{\rho j} P_j \jmath_1,$$

$$\Xi_2 = \jmath_1^*(J_1 + J_2)\jmath_1 - (1-\mu)e^{-\alpha\partial_1}\jmath_2^* J_1 \jmath_2 \quad - e^{-\alpha\partial_1}\jmath_3^* J_2 \jmath_3 + \jmath_4^* J_3 \jmath_4 - (1-\mu)e^{-\alpha\partial_1}\jmath_5^* J_3 \jmath_5,$$

$$\Xi_3 = \partial_1[\jmath_1\ \jmath_{10}]^* \mathscr{G}_1 [\jmath_1\ \jmath_{10}] + \partial_1^2 \jmath_{10}^* \mathscr{G}_2 \jmath_{10} + \jmath_1^* \mathscr{G}_m \jmath_1 \quad + \jmath_2^*(\mathscr{G}_n - \mathscr{G}_m)\jmath_2 + sym(\hat{J}_1\Omega_1 + \hat{J}_2\Omega_2)$$
$$+ \left(\frac{\partial_{1t}}{\partial_1} + \frac{\partial^2(t)}{\partial_1^2}\right) sym[\hat{Y}_1^* \hat{\varsigma}_1 + \hat{Y}_2^* \hat{\varsigma}_2] \quad + \jmath_3^* \mathscr{G}_n \jmath_3 - \left(\frac{\partial_{1t}}{\partial_1^2}\hat{\varsigma}_1^* \mathscr{G}_2 \hat{\varsigma}_1 + \frac{\partial(t)}{\partial_1^2}\hat{\varsigma}_2^* \mathscr{G}_2 \hat{\varsigma}_2\right),$$

$$\Xi_4 = e^{-\alpha h_2}\{h_2 \jmath_1^*[h_2 H_{11} + 2H_{13}^*]\jmath_1 \quad + 2\jmath_1^*[h_2 H_{12} - H_{13} + H_{23}^*]\jmath_{12}$$
$$+ \jmath_{12}^*[h_2 H_{22} - 2H_{23}^*]\jmath_{12} + \jmath_{10}^* \quad \{h_2^2 \mathscr{G}_3 + d_2^2 \mathscr{G}_4\}\jmath_{10}\} + e^{-\alpha d_2}\{-(\jmath_1 - \jmath_{14})^* \times \{\mathscr{G}_4(\jmath_1 - \jmath_{14}) + \mathscr{K}_1(\jmath_{14} - \jmath_{15})\}$$
$$- (\jmath_{14} - \jmath_{15})^* \mathscr{G}_4(\jmath_{14} - \jmath_{15})\} - e^{-\alpha h_2}\{\jmath_1^* \tilde{\mathscr{G}}_3 \jmath_1 \quad + \jmath_1^* \tilde{\mathscr{G}}_3 \jmath_{11} - \jmath_{11}^* 2\tilde{\mathscr{G}}_3 \jmath_{11} + \jmath_{11}^* \tilde{\mathscr{G}}_3 \jmath_{12} - \jmath_{12}^* \tilde{\mathscr{G}}_3 \jmath_{12}\},$$

$$\Xi_5 = -\jmath_1^* \hat{X}_1 \hat{\Lambda}_1 \jmath_1 + \jmath_1^* \hat{X}_2 \hat{\Lambda}_1 \jmath_4 - \jmath_4^* \hat{\Lambda}_1 \jmath_4 - \jmath_2^* \hat{X}_1 \hat{\Lambda}_2 \jmath_2 \quad + \jmath_2^* \hat{X}_2 \hat{\Lambda}_2 \jmath_5 - \jmath_5^* \hat{\Lambda}_2 \jmath_5 \quad - \jmath_{14}^* \mathcal{V} \bar{\phi}_g^- \jmath_{14}$$
$$+ \jmath_{14}^* \mathcal{V} \bar{\phi}_g^+ \jmath_{16} - \jmath_{16}^* \mathcal{V} \jmath_{14},$$

$$\Xi_6 = Sym\Big[\jmath_1^* \mathscr{W}_1 + \jmath_{10}^* \mathscr{W}_2 + \jmath_4^* \mathscr{W}_3 + \jmath_5^* \mathscr{W}_4\Big]\Big[- \jmath_{10} - \bar{M}_\rho \jmath_1 + \bar{N}_\rho \jmath_4 + \bar{O}_\rho \jmath_5$$
$$+ \bar{\beta} K_\rho[\jmath_{11} + \jmath_{13}] + (1-\bar{\beta})K_\rho \jmath_{16} + E_\rho \jmath_{17} + \bar{\beta}(1-\bar{\beta}) \times K_\rho[\jmath_{14} + \jmath_{13} - \jmath_{16}]\Big],$$

$$\Xi_7 = \phi \jmath_{11}^* \Theta_\rho \jmath_{11} - \jmath_{13}^* \Theta_\rho \jmath_{13}, \ \tilde{\Xi}_{11} = \jmath_{17}^* \frac{-\alpha}{\hat{w}^2} I \jmath_{17},$$

$$\tilde{\Psi}_{12} = \sqrt{\partial_1}\hat{J}_2^*, \ \tilde{\Psi}_{13} = \sqrt{\partial_1}\hat{Y}_2^*, \ \tilde{\Psi}_{22} = -e^{-\alpha\partial_1}\tilde{\mathscr{G}}_n,$$
$$\tilde{\Psi}_{33} = -e^{-\alpha\partial_1}\mathscr{G}_2,$$
$$\bar{\Psi}_{12} = \sqrt{\partial_1}\hat{J}_1^*, \ \bar{\Psi}_{13} = \sqrt{\partial_1}\hat{Y}_1^*, \ \bar{\Psi}_{22} = -e^{-\alpha\partial_1}\tilde{\mathscr{G}}_m,$$
$$\bar{\Psi}_{33} = -e^{-\alpha\partial_1}\mathscr{G}_2,$$

then, for any time-varying delay satisfying (2), the reachable set is bounded by $\epsilon(P_\rho) = \{r(t) \in \mathbb{C}^n | r^*(t) P_\rho r(t) \le 1\}$.

Proof Construct the LKF for the system (10) as

$$V(r_t) = V_1(r_t) + V_2(r_t) + V_3(r_t) + V_4(r_t), \tag{17}$$

where

$$V_1(r_t) = r^*(t) P_\rho r(t),$$
$$V_2(r_t) = \int_{t-\partial(t)}^{t} e^{\alpha(s-t)} r^*(s) J_1 r(s) \mathrm{d}s + \int_{t-\partial_1}^{t} e^{\alpha(s-t)} r^*(s) J_2 r(s) \mathrm{d}s + \int_{t-\partial(t)}^{t} e^{\alpha(s-t)} f^*(r(s)) J_3 f(r(s)) \mathrm{d}s,$$
$$V_3(r_t) = \int_{t-\partial_1}^{t} \int_{\theta}^{t} e^{\alpha(s-t)} \mho^*(s) \mathscr{G}_1 \mho(s) \mathrm{d}s d\theta + \int_{t-\partial_1}^{t} \int_{\theta}^{t} e^{\alpha(s-t)} \dot{r}^*(s) \mathscr{G}_2 \dot{r}(s) \mathrm{d}s d\theta,$$
$$V_4(r_t) = h_2 \int_{-h_2}^{0} \int_{t+\theta}^{t} e^{\alpha(s-t)} \dot{r}^*(s) \mathscr{G}_3 \dot{r}(s) \mathrm{d}s d\theta + d_2 \int_{-d_2}^{0} \int_{t+\theta}^{t} e^{\alpha(s-t)} \dot{r}^*(s) \mathscr{G}_4 \dot{r}(s) \mathrm{d}s d\theta. \tag{18}$$

Let $\mathcal{L}(.)$ be the weak infinitesimal generator of $\{r(t), e_t, t \ge 0\}$, then through some simple calculations, we yield

$$\mathcal{L}V_1(r_t) = 2r^*(t) P_\rho \dot{r}(t) + r^*(t) \sum_{j=1}^{N} \Pi_{\rho j} P_j r(t), = \chi^*(t) \Xi_1 \chi(t) - \alpha V_1(t), \tag{19}$$

$$\mathcal{L}V_2(r_t) \le r^*(t)(J_1 + J_2) r(t) - e^{-\alpha\partial_1}\{(1-\mu) r^*(t - \partial(t)) J_1 r(t - \partial(t)) + r^*(t - \partial_1) J_2 r(t - \partial_1)$$
$$- (1-\mu) f^*(r(t - \partial(t))) J_3 f(r(t - \partial(t)))\} + f^*(r(t)) J_3 f(r(t)) - \alpha V_2(t),$$

$$= \chi^*(t)\Xi_2\chi(t) - \alpha V_2(t), \tag{20}$$

$$\begin{aligned}\mathcal{L}V_3(r_t) &= \partial_1\mho^*(t)\mathscr{G}_1\mho(t) - \int_{t-\partial_1}^{t} e^{\alpha(s-t)}\mho^*(\theta)\mathscr{G}_1\mho(\theta)d\theta + \partial_1\dot{r}^*(t)\mathscr{G}_2\dot{r}(t)\\ &\quad - \int_{t-\partial_1}^{t} e^{\alpha(s-t)}\dot{r}^*(\theta)\mathscr{G}_2\dot{r}(\theta)d\theta,\\ &\le e^{2\alpha(-\partial_1)}\{e^{2\alpha\partial_1}(\partial_1\mho^*(t)\mathscr{G}_1\mho(t) + \partial_1\dot{r}^*(t)\mathscr{G}_2\dot{r}(t))\}\\ &\quad - e^{-\alpha\partial_1}\int_{t-\partial_1}^{t}\mho^*(\theta)\mathscr{G}_1\mho(\theta)d\theta - e^{-\alpha\partial_1}\int_{t-\partial_1}^{t}\dot{r}^*(\theta)\mathscr{G}_2\dot{r}(\theta)d\theta - \alpha V_3(t).\end{aligned} \tag{21}$$

Before bounding those integrals in (21), the following zero-value equalities are considered, which were reported in [50]:

$$0 = e^{-\alpha\partial_1}[r^*(t)\mathscr{G}_m r(t) - r^*(t-\partial(t))\mathscr{G}_m r(t-\partial(t))] - 2e^{-\alpha\partial_1}\int_{t-\partial(t)}^{t} r^*(s)\mathscr{G}_m\dot{r}(s)\mathrm{d}s, \tag{22}$$

$$0 = e^{-\alpha\partial_1}[r^*(t-\partial(t))\mathscr{G}_n r(t-\partial(t)) - r^*(t-\partial_1)\mathscr{G}_n r(t-\partial_1)] - 2e^{-\alpha\partial_1}\int_{t-\partial_1}^{t-\partial(t)} r^*(s)\mathscr{G}_n\dot{r}(s)\mathrm{d}s. \tag{23}$$

Adding (22) and (23) into (21), we get

$$\mathcal{L}V_3(r_t) = \chi^*(t)\nabla_4\chi(t) + e^{-\alpha\partial_1}(-\varphi_1 - \varphi_2) - \alpha V_3(t), \tag{24}$$

where

$$\varphi_1 = \int_{t-\partial(t)}^{t}\mho^*(\theta)\hat{\mathscr{G}}_m\mho(\theta)d\theta + \int_{t-\partial_1}^{t-\partial(t)}\mho^*(\theta)\hat{\mathscr{G}}_n\mho(\theta)d\theta, \tag{25}$$

$$\varphi_2 = -\int_{t-\partial_1}^{t}\dot{r}^*(\theta)\mathscr{G}_2\dot{r}(\theta)d\theta, \tag{26}$$

$$\begin{aligned}\nabla_4 &= \partial_1[\jmath_1\ \jmath_{10}]^*\mathscr{G}_1[\jmath_1\ \jmath_{10}] + \partial_1\jmath_{10}^*\mathscr{G}_2\jmath_{10} + \jmath_1^*\mathscr{G}_m\jmath_1 + \jmath_3^*\mathscr{G}_n\jmath_3 + \jmath_2^*(\mathscr{G}_n - \mathscr{G}_m)\jmath_2,\\ \hat{\mathscr{G}}_m &= \mathscr{G}_1 + \begin{bmatrix}0 & \mathscr{G}_m\\ \star & 0\end{bmatrix},\ \ \hat{\mathscr{G}}_n = \mathscr{G}_1 + \begin{bmatrix}0 & \mathscr{G}_n\\ \star & 0\end{bmatrix}.\end{aligned} \tag{27}$$

Utilizing Lemma 2 and 3, φ_1 and φ_2 can be written as

$$\begin{aligned}\bar{\varphi}_1 &= \chi^*(t)\{\partial(t)\hat{J}_1^*\tilde{\mathscr{G}}_m^{-1}\hat{J}_1 + \partial_{1t}\hat{J}_2^*\tilde{\mathscr{G}}_n^{-1}\hat{J}_2 + sym(\hat{J}_1\Omega_1 + \hat{J}_2\Omega_2)\}\chi(t),\\ \varphi_2 &\le \chi^*(t)[\partial(t)\hat{Y}_1^*\mathscr{G}_2^{-1}\hat{Y}_1 + \partial_{1t}\hat{Y}_2^*\mathscr{G}_2^{-1}\hat{Y}_2 + \left(\frac{\partial_{1t}}{\partial_1} + \frac{(\partial(t))^2}{\partial_1^2}\right)sym[\hat{Y}_1^*\hat{\varsigma}_1 + \hat{Y}_2^*\hat{\varsigma}_2] - \left(\frac{\partial_{1t}}{\partial_1^2}\hat{\varsigma}_1^*\mathscr{G}_2\hat{\varsigma}_1 + \frac{\partial(t)}{\partial_1^2}\hat{\varsigma}_2^*\mathscr{G}_2\hat{\varsigma}_2\right)]\chi(t),\\ \mathcal{L}V_3(r_t) &\le \chi^*(t)[\nabla_4 + \bar{\varphi}_1 + \hat{\Theta}_{01}(\partial(t)) + \Theta_{01}(\partial(t))]\chi(t) - \alpha V_3(t),\\ \mathcal{L}V_3(r_t) &\le \chi^*(t)\Xi_3\chi(t) - \alpha V_3(t),\end{aligned} \tag{28}$$

$$\mathcal{L}V_4(r_t) \le h_2^2\dot{r}^*(t)\mathscr{G}_3\dot{r}(t) - h_2\int_{t-h_2}^{t} e^{\alpha(s-t)}\dot{r}^*(s)\mathscr{G}_3\dot{r}(s)\mathrm{d}s + d_2^2\dot{r}^*(t)\mathscr{G}_4\dot{r}(t) - d_2\int_{t-d_2}^{t} e^{\alpha(s-t)}\dot{r}^*(s)\mathscr{G}_4\dot{r}(s)\mathrm{d}s - \alpha V_4(t). \tag{29}$$

The integral term in (29) can be rewritten as

$$-h_2\int_{t-h_2}^{t} e^{\alpha(s-t)}\dot{r}^*(s)\mathscr{G}_3\dot{r}(s)\mathrm{d}s - e^{-\alpha h_2}\{h_2\int_{t-h_2}^{t}\dot{r}^*(s)[\mathscr{G}_3 - H_{33}]\dot{r}(s)\mathrm{d}s - h_2\int_{t-h_2}^{t}\dot{r}^*(s)H_{33}\dot{r}(s)\mathrm{d}s\}. \tag{30}$$

By utilizing Lemma 4 and Leibniz–Newton formula for any matrix $H_{ij} > 0$, $(i, j = 1, 2, 3)$, we obtain

$$-h_2\int_{t-h_2}^{t}\dot{r}^*(s)H_{33}\dot{r}(s)\mathrm{d}s \le h_2 r^*(t)[h_2H_{11} + 2H_{13}^*]r(t) + 2r^*(t)$$

$$\times [h_2 H_{12} - H_{13} + H_{23}^*] r(t-h_2) + r^*(t-h_2)[h_2 H_{22} - 2H_{23}^*] r(t-h_2). \tag{31}$$

Let $\tilde{\mathscr{G}}_3 = \mathscr{G}_3 - H_{33}$ and with reference to Lemma 2.5 in [51], the integral term in (30) can be rewritten as

$$-h_2 \int_{t-h_2}^{t} \dot{r}^*(s)[\mathscr{G}_3 - H_{33}]\dot{r}(s)\mathrm{d}s \le \nu^*(t) \begin{bmatrix} -\tilde{\mathscr{G}}_3 & \tilde{\mathscr{G}}_3 & 0 \\ \star & -2\tilde{\mathscr{G}}_3 & \tilde{\mathscr{G}}_3 \\ \star & \star & -\tilde{\mathscr{G}}_3 \end{bmatrix} \nu(t).$$

Utilizing the reciprocal convex inequality technique, the following inequalities hold if there exist $\mathscr{K}_1$ satisfying (14):

$$-d_2 \int_{t-d_2}^{t} \dot{r}^*(s)\mathscr{G}_4\dot{r}(s)\mathrm{d}s \le -\begin{bmatrix} r(t) - r(t_{d(t)}) \\ r(t_{d(t)}) - r(t_{d_2}) \end{bmatrix}^* \begin{bmatrix} \mathscr{G}_4 & \mathscr{K}_1 \\ \star & \mathscr{G}_4 \end{bmatrix} \begin{bmatrix} r(t) - r(t_{d(t)}) \\ r(t_{d(t)}) - r(t_{d_2}) \end{bmatrix}, \tag{32}$$

$$\mathcal{L}V_4(r_t) \le \chi^*(t)\Xi_4\chi(t) - \alpha V_4(t). \tag{33}$$

where $\nu(t) = [r^*(t)\ r^*(t-\eta(t))\ r^*(t-h_2)]^*$, $r(t_{d(t)}) = r(t-d(t))$, $r(t_{d_2}) = r(t-d_2)$.

Depending on the activation function, we have

$$[f_s(r_s(t)) - \hat{X}_s^- r_s(t)][f_s(r_s(t)) - \hat{X}_s^+ r_s(t)] \le 0,\ [f_s(r_s(t-\partial(t))) - \hat{X}_s^- r_s(t-\partial(t))] \times [f_s(r_s(t-\partial(t))) - \hat{X}_s^+ r_s(t-\partial(t))] \le 0,\ \ s = 1, 2, ..., n.$$

For any $n \times n$ diagonal matrices $\hat{\Lambda}_1 > 0$, $\hat{\Lambda}_2 > 0$. Then, the above condition can be written as

$$\begin{aligned} &\begin{bmatrix} r(t) \\ f(r(t)) \end{bmatrix}^* \begin{bmatrix} \hat{X}_1\hat{\Lambda}_1 & -\hat{X}_2\hat{\Lambda}_1 \\ \star & \hat{\Lambda}_1 \end{bmatrix} \begin{bmatrix} r(t) \\ f(r(t)) \end{bmatrix} &&\le 0, \\ &\begin{bmatrix} r(t-\partial(t)) \\ f(r(t-\partial(t))) \end{bmatrix}^* \begin{bmatrix} \hat{X}_1\hat{\Lambda}_2 & -\hat{X}_2\hat{\Lambda}_2 \\ \star & \hat{\Lambda}_2 \end{bmatrix} \begin{bmatrix} r(t-\partial(t)) \\ f(r(t-\partial(t))) \end{bmatrix} &&\le 0. \end{aligned} \tag{34}$$

From Assumption 2, it is not difficult to know that there exist $\mathcal{V}$ such that

$$\begin{bmatrix} r(t_{d(t)}) \\ g(r(t_{d(t)})) \end{bmatrix}^* \begin{bmatrix} \mathcal{V}\bar{\phi}_g^- & -\mathcal{V}\bar{\phi}_g^+ \\ \bar{\phi}_g^+\mathcal{V} & \mathcal{V} \end{bmatrix} \begin{bmatrix} r(t_{d(t)}) \\ g(r(t_{d(t)})) \end{bmatrix} \le 0. \tag{35}$$

Combining (34) and (35), we get

$$\chi^*(t)\Xi_5\chi(t) \le 0. \tag{36}$$

In addition, for any real matrix $\mathscr{W}_l (l = 1, 2, 3, 4)$, we have the following inequalities:

$$\begin{aligned} 0 = {} & Sym\Big[r^*(t)\mathscr{W}_1 + \dot{r}^*(t)\mathscr{W}_2 + f^*(r(t))\mathscr{W}_3 + f^*(r(t-\partial(t)))\mathscr{W}_4\Big] \\ & \times \Big[-\dot{r}(t) - \bar{M}_\rho r(t) + \bar{N}_\rho f(r(t)) + \bar{O}_\rho f(r(t-\partial(t))) + \bar{\beta}K_\rho[r(t-\eta(t)) + \tilde{e}(t)] + (1-\bar{\beta})K_\rho g(r(t-d(t))) \\ & + E_\rho w(t) + \bar{\beta}(1-\bar{\beta})K_\rho[r(t-\eta(t)) + \tilde{e}(t) - g(r(t-d(t)))]\Big], \\ 0 = {} & \chi^*(t)\Xi_6\chi(t). \end{aligned} \tag{37}$$

With the help of Schur complement Lemma, (12), and (19)–(37), it can derived that

$$\mathcal{L}V(r_t) + \alpha V(r_t) - \frac{\alpha}{\hat{w}^2} w^*(t)w(t) < \chi^*(t)\tilde{\Psi}_{[\partial(t)]}\chi(t) < 0. \tag{38}$$

This demonstrates that the proposed CVNNs is stable. Based on Lemma 1, which can be verify that $r^*(t)P_\rho r(t) \le 1$, as a result (10) can be bounded by $\epsilon(P_\rho)$. □

Theorem 2 For given an ET controller (6) and scalars, ∂_1, μ, h_2, d_2, ϕ, $k_l(l = 1, 2, 3, 4)$, and constant $\alpha > 0$, if there exist matrices $\tilde{P} > 0 \in \mathbb{R}^n$ and $\tilde{J}_1 > 0$, $\tilde{J}_i > 0$, $\tilde{\mathscr{G}}_1 \in \mathbb{C}^{2n\times 2n} > 0$, $\tilde{\mathscr{G}}_i > 0(i = 2, 3, 4)$, $\tilde{\mathscr{G}}_m > 0$, $\tilde{\mathscr{G}}_n > 0$, $\mathbb{W} > 0$, $\tilde{\mathscr{K}}_1$ being Hermitian, positive diagonal matrices $\hat{\Lambda}_r > 0(r = 1, 2)$, and appropriate dimensional matrices $\tilde{\mathscr{S}}_i \in \mathbb{C}^{7n\times 4n}$, $(i = 1, 2)$, $\tilde{\hat{Y}}_1$, $\tilde{\hat{Y}}_2$, $\tilde{\Theta} > 0$, such that

$$\begin{bmatrix} \tilde{\mathscr{G}}_4 & \tilde{\mathscr{K}}_1 \\ \star & \tilde{\mathscr{G}}_4 \end{bmatrix} \geq 0 \tag{39}$$

$$\begin{bmatrix} \tilde{\Sigma}_{[\partial(t)=0]} & \tilde{\Sigma}_{12} & \tilde{\Sigma}_{13} \\ \star & \tilde{\Sigma}_{22} & 0 \\ \star & \star & \tilde{\Sigma}_{33} \end{bmatrix} < 0 \tag{40}$$

$$\begin{bmatrix} \hat{\Sigma}_{[\partial(t)=\partial_1]} & \hat{\Sigma}_{12} & \hat{\Sigma}_{13} \\ \star & \hat{\Sigma}_{22} & 0 \\ \star & \star & \hat{\Sigma}_{33} \end{bmatrix} < 0 \tag{41}$$

are fulfilled, then the system described in (10) is synchronous, as a result $\epsilon(P) = \{r(t) \in \mathbb{R}^n | r^*(t)Pr(t) \leq 1\}$. Additionally, the appropriate gain matrices are provided by $K_\rho = \mathbb{Y}_\rho \bar{\mathbb{W}}^{-1}$ and other terms in the LMIs have been defined in Appendix A.

Proof Following the same proof procedure as in Theorem 1 and define $\mathscr{W}_i = k_i\mathbb{W}$ $(i = 1, 2, 3, 4)$, $\bar{\mathbb{W}} = \mathbb{W}^{-1}$, $\mathbb{Y}_\rho = K_\rho\bar{\mathbb{W}}$, $\tilde{\Theta}_0 = \{\bar{\mathbb{W}}^*, \bar{\mathbb{W}}^*\}$, $\tilde{\Theta}_1 = \{\underbrace{\bar{\mathbb{W}}^*, \bar{\mathbb{W}}^*, \ldots, \bar{\mathbb{W}}^*}_{7\ times}\}$, $\tilde{\Theta}_2 = diag\{\tilde{\Theta}_0, \tilde{\Theta}_1, \tilde{\Theta}_1, I, \bar{\mathbb{W}}^*, \bar{\mathbb{W}}^*\}$, $\tilde{P} = \bar{\mathbb{W}}^*P\bar{\mathbb{W}}$, $\tilde{J}_i = \bar{\mathbb{W}}^*J_i\bar{\mathbb{W}}$, $\tilde{\mathscr{G}}_i = \bar{\mathbb{W}}^*\mathscr{G}_i\bar{\mathbb{W}}$, $(i = 1, 2, 3, 4)$, $\tilde{\mathscr{G}}_m = \bar{\mathbb{W}}^*\mathscr{G}_m\bar{\mathbb{W}}$, $\tilde{\mathscr{G}}_n = \bar{\mathbb{W}}^*\mathscr{G}_n\bar{\mathbb{W}}$, $\tilde{\mathscr{S}}_i = \bar{\mathbb{W}}^*\mathscr{S}_i\bar{\mathbb{W}}$, $\tilde{H}_{11} = \bar{\mathbb{W}}^*H_{11}\bar{\mathbb{W}}$, $\tilde{H}_{12} = \bar{\mathbb{W}}^*H_{12}\bar{\mathbb{W}}$, $\tilde{H}_{13} = \bar{\mathbb{W}}^*H_{13}\bar{\mathbb{W}}$, $\tilde{H}_{22} = \bar{\mathbb{W}}^*H_{22}\bar{\mathbb{W}}$, $\tilde{H}_{23} = \bar{\mathbb{W}}^*H_{23}\bar{\mathbb{W}}$, $\tilde{K}_1 = \bar{\mathbb{W}}^*K_1\bar{\mathbb{W}}$, $\tilde{\Theta} = \bar{\mathbb{W}}^*\Theta\bar{\mathbb{W}}$. Pre- and post-multiplying (15) and (16) by $\tilde{\Theta}_2$ and $\tilde{\Theta}_2^*$, we get (40), and (41). This completes the proof. □

Remark 2 Generally, synchronization schemes with event-triggered control (ETC), reachable set estimation, and Markovian jumping problems are not simply applied to complex-valued neural networks (CVNNs) under cyber-attacks, some research publications have tackled such problems. It is noted that the authors of [26,30] investigated the ETC and impulsive control problem for synchronization for complex-valued memristive neural networks in the presence of delays. Moreover, the work presented in [27] explored the event-based synchronization for CVNNs with pinning impulsive control. Further, in [36,37], the authors explored the reachable set estimation for delayed memristive CVNNs with some disturbances. The model considered in the present study is more practical than that proposed by [26,27,30,36,37] because they consider usual ETC has been studied with CVNNs based on stabilization conditions, but we consider ETC, with the combination of synchronization approach, reachable set estimation, cyber-attacks, and Markovian jumping modes. Due to the many real-life applications the combined study of Markovian jump CVNNs and ETC to the system model is more important. The purpose of this study is to establish synchronization conditions of these complex networks by applying the Lyapunov functional theory and event-triggered communication scheme and to apply a practical application of image encryption and decryption. In event-triggered control, the measured error plays a key role during the event-triggered controller design. An event will be triggered to update the event-triggered controller when its magnitude reaches the prescribed value. Additionally, it is mentioned that we utilize composite slack-matrix-based inequality techniques and some novel zero equations to estimate the derivative of a Lyapunov functional, such as defined in $\mathcal{L}V_3(r_t)$ which can induce tighter information on the delay of the considered system. Hence, the comprehensive analysis of the proposed control strategy in the presence of multiple challenges demonstrates the system's relevance and applicability to real-world scenarios.

4 Simulation example

In this section, CVNNs simulation examples are provided under the ET technique with cyberattack and reachable set analysis to evaluate the theoretical results. We take into account a CVNN that has two neurons of complex value.

Example 1 Consider the system (10) with two jumping modes ($\rho = 1, 2$) and the following matrix values are characterized as follows:

Mode 1:

$$\bar{M}_1 = \begin{bmatrix} 2 & 0 \\ 0 & 2 \end{bmatrix}, \ \bar{N}_1 = \begin{bmatrix} 0.1+0.2i & 1.1+2i \\ 0.2-0.3i & 1.2+0.3i \end{bmatrix}, \bar{O}_1 = \begin{bmatrix} 0.1-0.4i & 0.1-0.5i \\ 0.2+0.2i & 0.3-0.7i \end{bmatrix}, \ E_1 = \begin{bmatrix} 0.1 & 0 \\ 0 & 0.1 \end{bmatrix}.$$

Mode 2:

$$\bar{M}_1 = \begin{bmatrix} 2.5 & 0 \\ 0 & 3 \end{bmatrix}, \ \bar{N}_1 = \begin{bmatrix} 0.15+0.3i & 1.2+2i \\ 0.3-0.3i & 0.2+0.4i \end{bmatrix}, \bar{O}_1 = \begin{bmatrix} 0.3-0.5i & 0.3-0.5i \\ 0.3+0.2i & 0.2-0.4i \end{bmatrix}, \ E_1 = \begin{bmatrix} 0.2 & 0 \\ 0 & 0.2 \end{bmatrix}.$$

The activation functions are set to $f(r(\cdot)) = \tanh(r(\cdot))$, and the cyber-attack function is assumed to be $g(r) = \begin{bmatrix} \tanh(0.04r_1(t)) \\ \tanh(0.04r_2(t)) \end{bmatrix}$. Moreover, the transition probability matrix is chosen as $\Pi = \begin{bmatrix} -2 & 2 \\ 5 & -5 \end{bmatrix}$. One concludes that there is a real-valued diagnostic matrix by the use of direct calculation, then we get $\hat{X}_1 = 0$, $\hat{X}_2 = diag\{0.5, 0.5\}$, $\bar{\phi}_g^- = diag\{0, 0\}$, $\bar{\phi}_g^+ = diag\{0.02, 0.02\}$, to satisfy Assumptions 1 and 2. In the following, we examine two neural network scenarios. In Case A, a neural network is applied to both the event-triggered scheme and cyberattacks. In Case B, a neural network employs the event-triggered approach without cyber-attacks.

Case A: Assume that $\partial(t) = 0.1\sin t + 0.2$. It is easy to see that $\partial_1 = 0.3$, $\mu = 0.1$, $\bar{\beta} = 0.5$, $d_2 = 0.2$. We take into account the modeled ETM (5) for the error system (10). Without loss of generality, the trigger parameters are assumed to be $h_2 = 0.2$, $\phi = 0.1$. Using the YALMIP toolbox in MATLAB, a set of feasible solutions to the LMIs (40)-(41) is determined, and ultimately, the controller gains and triggered matrices can be obtained as follows:

$$K_1 = \begin{bmatrix} 0.6999+0.0113i & -0.0645+0.0152i \\ -0.0379-0.0297i & 0.8183-0.0113i \end{bmatrix}, K_2 = \begin{bmatrix} 1.0356-0.0036i & -0.0048-0.0957i \\ -0.0218+0.1600i & 0.6660+0.0036i \end{bmatrix},$$
$$\Theta_1 = \begin{bmatrix} 2.7768+0.0000i & -0.0165-0.0150i \\ -0.0165+0.0150i & 2.7563+0.0000i \end{bmatrix}, \Theta_2 = \begin{bmatrix} 3.5193+0.0000i & 0.0129+0.0084i \\ 0.0129-0.0084i & 3.5280+0.0000i \end{bmatrix}.$$

Furthermore, the equivalent time responses of the system state $\mathrm{Re}(r(t))$ and $\mathrm{Im}(r(t))$ of the investigated master and slave systems are depicted in Fig. 1, respectively, with randomized initial values utilizing the aforementioned control gain matrix. It can be observed that the system states ultimately converge to zero. Figure 2 demonstrates the responses of the reachable set bounding with $w(t) = \sin(2t)$. Figure 3 shows the ET scheme release intervals, respectively, indicating the effectiveness and efficiency of the suggested theory. Based on the simulation process described above, we can see from Figs. 1 and 3 that using the ET controller can keep all the reachable states of the system within the ellipsoid region of the set. This solves the reachable set-synthesis problem. In other words, our suggested strategy has been proven to work.

Case B: When the neural network is operating under an event-triggered scheme but there are no active cyber-attacks, set the same parameters as follows in Case A: $\partial_1 = 0.3$, $\mu = 0.1$, $\bar{\beta} = 0.5$, $d_2 = 0.2$. Furthermore, the triggering parameters are assumed to be $h_2 = 0.2$, $\phi = 0.1$. Using Theorem 2 LMIs and the YALMIP toolbox in MATLAB, we can obtain the controller gain as well as the triggering matrix in the following way:

$$K_1 = \begin{bmatrix} 1.8147-0.0062i & -0.0042-0.1462i \\ -0.0339+0.2425i & 1.1794+0.0062i \end{bmatrix}, K_2 = \begin{bmatrix} 1.2235-0.0038i & -0.0221-0.1185i \\ -0.0522+0.2106i & 0.8158+0.0038i \end{bmatrix},$$
$$\Theta_1 = \begin{bmatrix} 3.2427+0.0000i & -0.0146-0.0490i \\ -0.0146+0.0490i & 3.2395+0.0000i \end{bmatrix}, \Theta_2 = \begin{bmatrix} 0.9672+0.0000i & 0.0013-0.0073i \\ 0.0013+0.0073i & 0.9686+0.0000i \end{bmatrix}.$$

From the theoretical perspective, the results of without cyber-attack functions are examined numerically as follows. Figure 4 depicts the time trajectories of the real and imaginary components of master and slave systems with controlling input and without cyberattack functions, which shows the effect of the cyberattack function implemented in our proposed network. Figure 5 shows the release intervals of the ET scheme. The simulation results in Figs. 1-5 for Cases A and B indicate satisfactory synchronization of master–slave CVNNs as defined by (1) both with and without cyber-attacks. From this analysis, the system stabilizes very fast and smoothly as the error plots are already shown in the Figure. Moreover, the effect of the cyberattack function that is implemented in our proposed system can be shown in Fig. 6 for both real and imaginary components. This shows that the cyberattack functions initially triggered the system, which is known as the sudden attack or intermittent attack of the networks. At the time of a cyber-attack, the network settles after some transients and exhibits a large variation from normal synchronizations.

Figure 7 shows the time trajectories of real and imaginary components of master and slave systems without controlling input, as well as cyberattack functions. From this analysis, the system does not stabilize and has

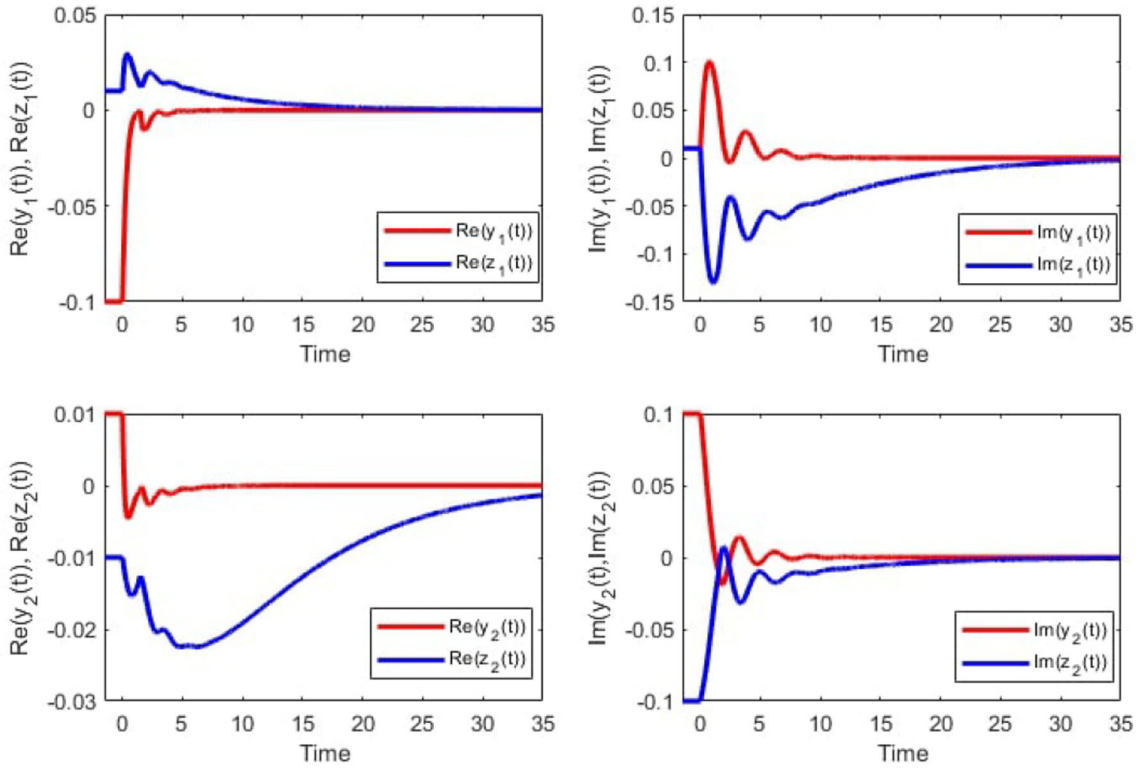

Fig. 1 Numerically computed time trajectories of real and imaginary components of master and slave systems with controlling input and cyberattack

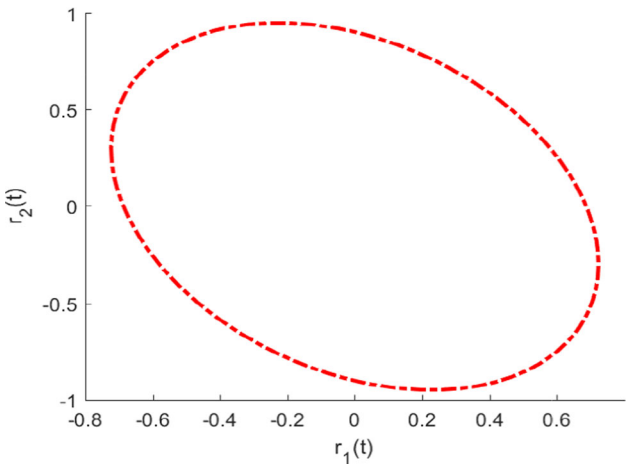

Fig. 2 Trajectories of the reachable set of the model (10) in Example 4.1

oscillations for a long time. From the conclusion of all the Figs. 1-7 results show that the master and slave system behavior is synchronized. These findings also show that the event-triggered scheme can stabilize the controlled system. The comprehensive approach of the graphical representations and the resulting conclusions demonstrate the importance of the established control mechanism in synchronizing and stabilizing.

5 Numerical results

The CVNNs (1) ($\mathscr{M}$) calculated using the Euler algorithm with a step size of 0.001, to obtain the dynamics. The choice of the Euler method over the more advanced Runge–Kutta (RK4) method in this study is primarily justified by the computational simplicity and efficiency it offers, especially for systems where high precision is not strictly

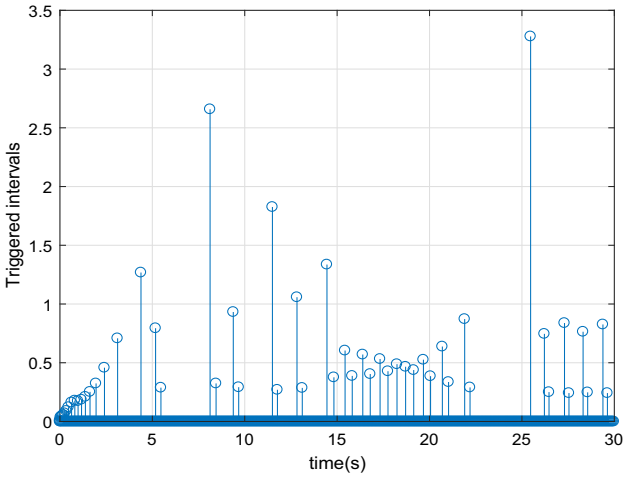

Fig. 3 Release intervals in case A

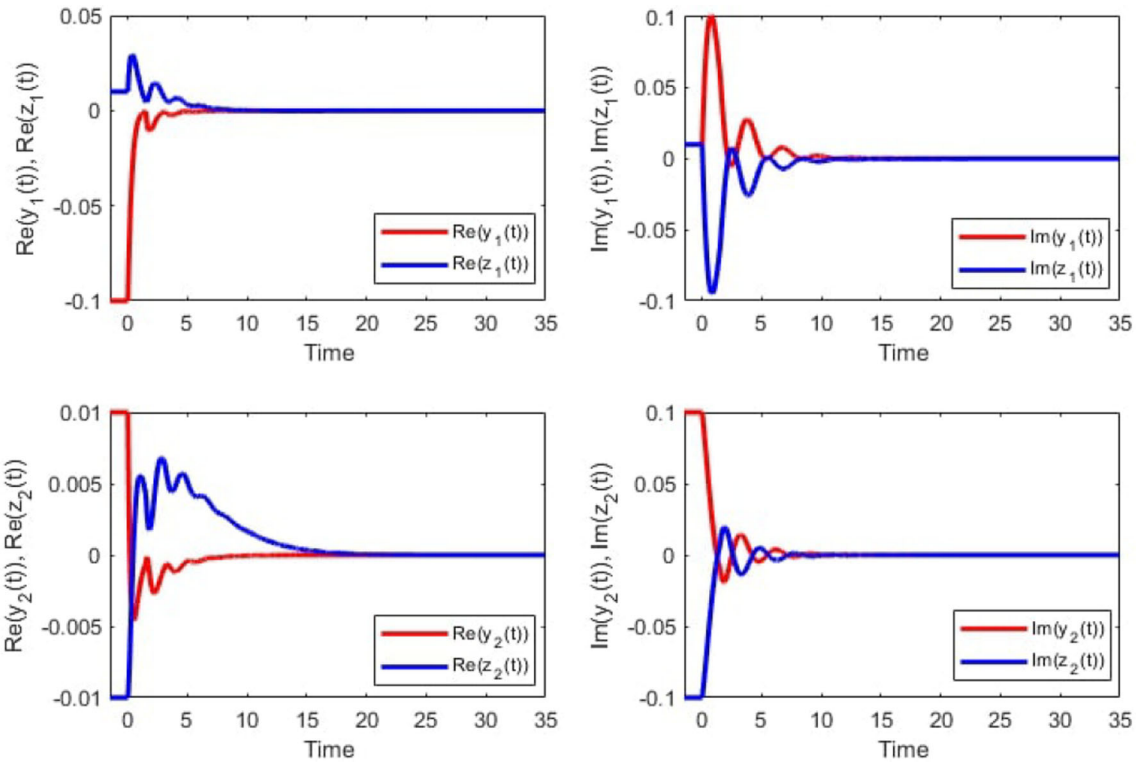

Fig. 4 Numerically computed time trajectories of real and imaginary components of master and slave systems with controlling input and without cyberattack functions

required. Although RK4 is known for its superior accuracy due to its higher-order error handling, it also involves more computational complexity, requiring multiple function evaluations per step. In contrast, the Euler method, though less accurate per step, allows for more efficient computations when paired with a sufficiently small step size, as used in our case (0.001). By reducing the step size, we effectively minimized truncation errors, achieving results comparable to RK4 while maintaining a lower computational overhead. This makes the Euler method a more practical choice for our purposes, where computational efficiency and simplicity are priorities, and the accuracy achieved through the reduced step size is sufficient for our analysis. Furthermore, we validated the results with RK4 and found no significant deviation, confirming the adequacy of the Euler method in this context. Figure 8 shows the chaotic oscillation of the CVNNs.

The phase portraits of real versus imaginary and real versus real parts of the master system, state variables $y_1(t)$, $y_2(t)$ are shown in 8a, b of the system (1). The corresponding times series of all the real and imaginary parts of the variables $y_1(t)$, $y_2(t)$ are also shown to confirm the presence of chaotic oscillations.

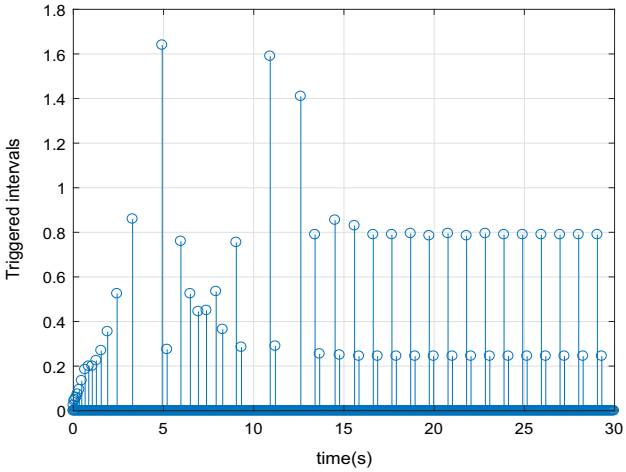

Fig. 5 Release intervals in case B

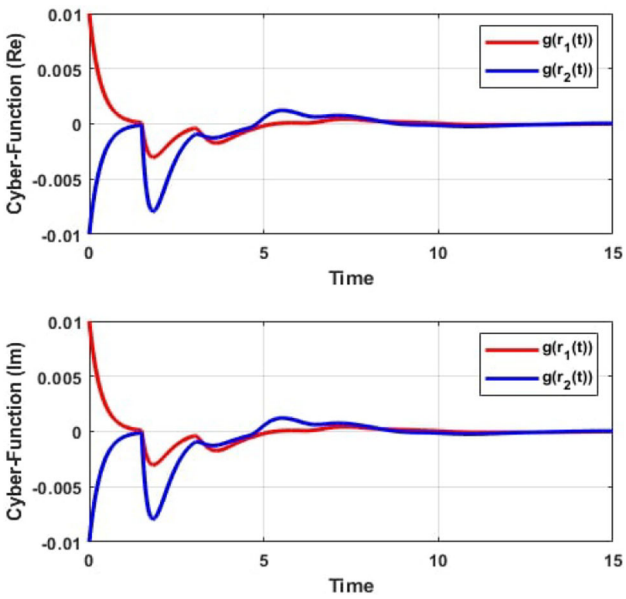

Fig. 6 Cyberattack functions of real and imaginary components

For visualizing the chaotic oscillation, Fig. 9 shows the three-dimensional phase space in the real part of the state variables $y_1(t)$, $y_2(t)$, and the imaginary part of the variable $y_1(t)$. The trajectories are visible and confirm the presence of chaotic oscillations due to their aperiodic nature are shown in the right hand side of Fig. 8.

Synchronizing a chaotic system poses challenges due to its sensitivity to initial conditions. Various synchronization methods have been proposed in the literature to address this issue when synchronizing two or more chaotic dynamical systems [28]. In this article, we employ a unidirectional synchronization scheme to synchronize CVNNs (10). Master of CVNNs is considered as $g(y(t))$ and slave as $g(z(t))$. Figure 10 shows the complete synchronization of both $(\mathscr{M})$ and $(\mathscr{S})$ of CVNNs. In the top panel, phase portraits are plotted in real parts of the $y_1(t)$ master and $z_1(t)$ slave systems. Similarly, the imaginary parts of $y_1(t)$ and $z_1(t)$ are plotted in the bottom panel. The time series are also plotted and indicate that the two-time trajectories are completely synchronized with phase and amplitude with a small transient.

5.1 Chaos communication

The importance and potential application of chaotic synchronization is to use the idea in the communication scenario. The main idea is for the information, whether it is a signal or image, to be masked with the chaotic signal as a key, which is a relatively low-volume signal. The masked signal is then sent to another system, which is identical to the master or the first chaotic system. Then only the information signal could be decrypted without loss of information. The other important point is to synchronize the chaotic system both in a unidirectional and bidirectional way to recover the original signal.

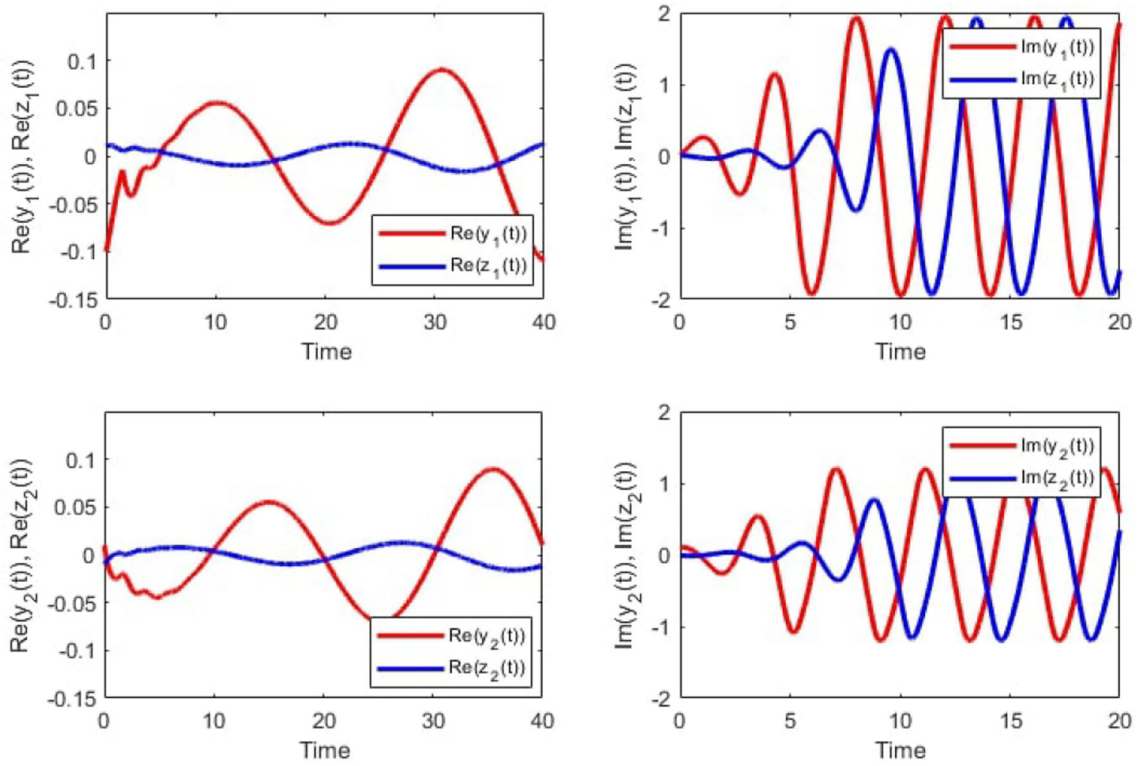

Fig. 7 Numerically computed time trajectories of real and imaginary components of master and slave systems without controlling input as well as cyber-attack functions

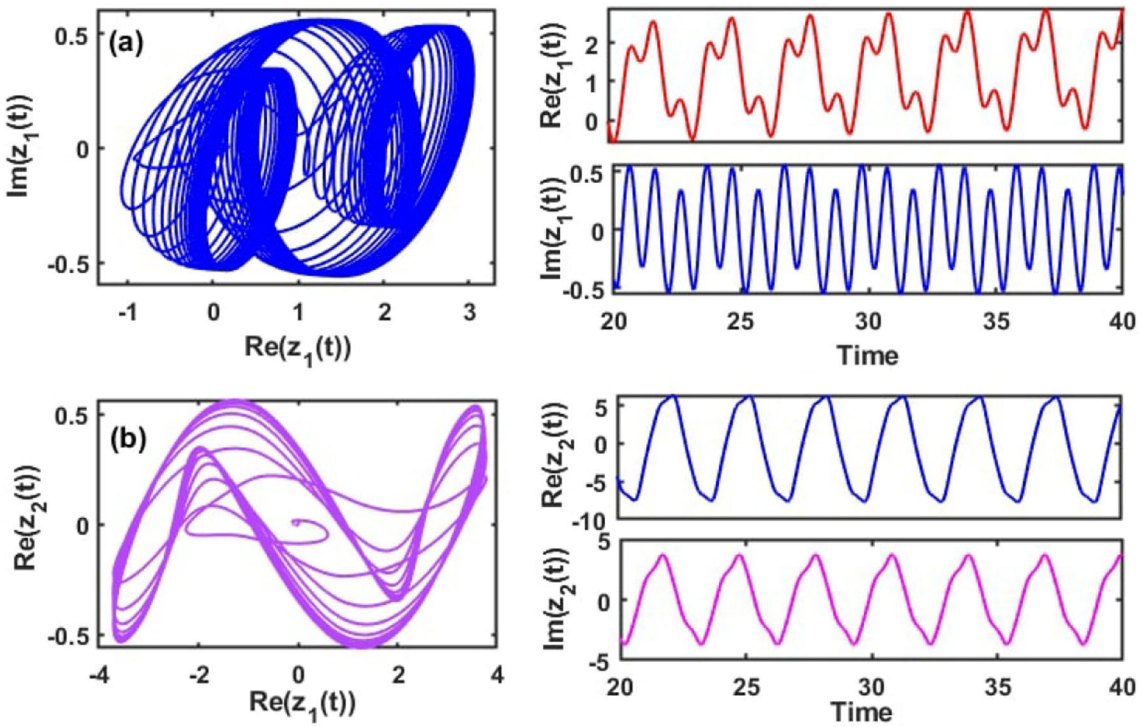

Fig. 8 Chaotic oscillations of CVNNs ($\mathscr{M}$) without control: **a** chaotic oscillation of the *Re* and *Im* parts of the ($\mathscr{M}$) system state variable $y_1(t)$, **b** *Re* parts of state variables $y_1(t)$, $y_2(t)$ and [right panels]: its corresponding time series of CVNNs (1)

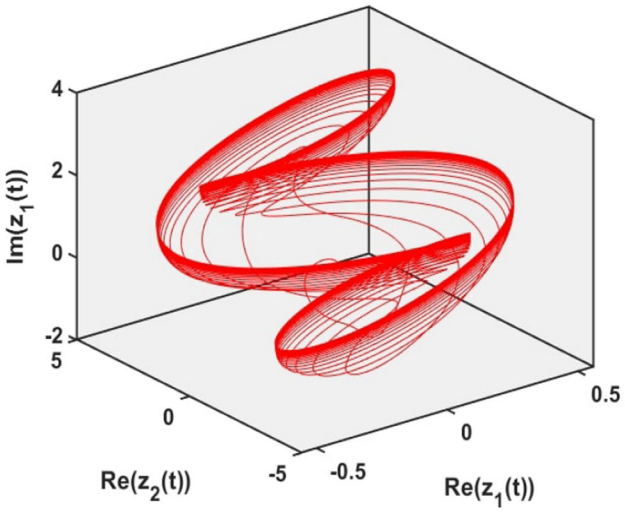

Fig. 9 Chaotic oscillations of CVNN without control of real part of state variables $y_1(t)$, $y_2(t)$ and imaginary part of $y_1(t)$ variable

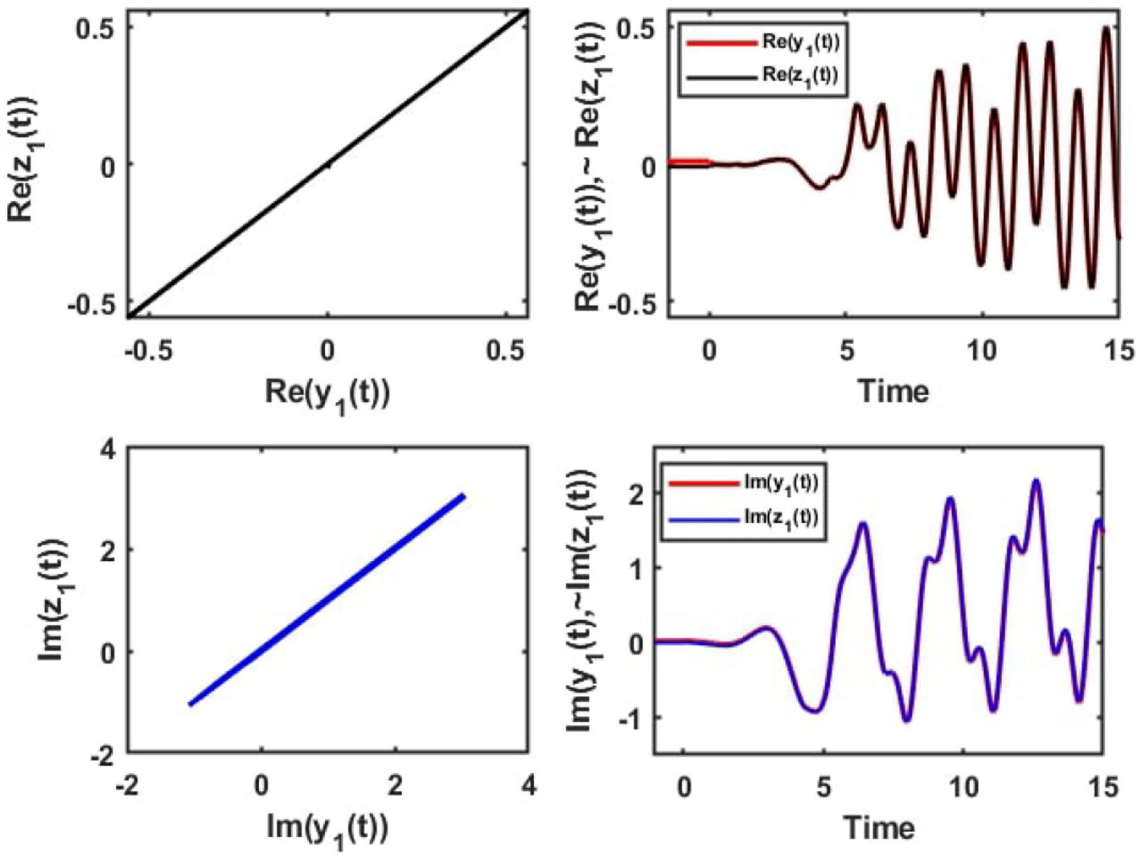

Fig. 10 Numerically computed synchronization of CVNNs (1), (left panel) phase portraits and (right panel) its corresponding time series. Black line represents $(y_1(t))$, and red line represents $(z_1(t))$. The error $e(t) = g(y(t)) - g(z(t))$ remains close to zero

Figure 11 shows the results of the chaotic communication scheme in our proposed CVNN model. The original input image and its corresponding fast Fourier transformed (FFT) plot are shown in Fig. 11a(i, ii). The encrypted image (modulated image mixed with chaotic signal) and its corresponding FFT are shown in Fig. 11b(i, ii), Finally, the recovered image with 99.4% similarity to the original image and its corresponding FFT are shown in Fig. 11c(i, ii). The following algorithms are used to achieve secure communication (image encryption) in the present system:

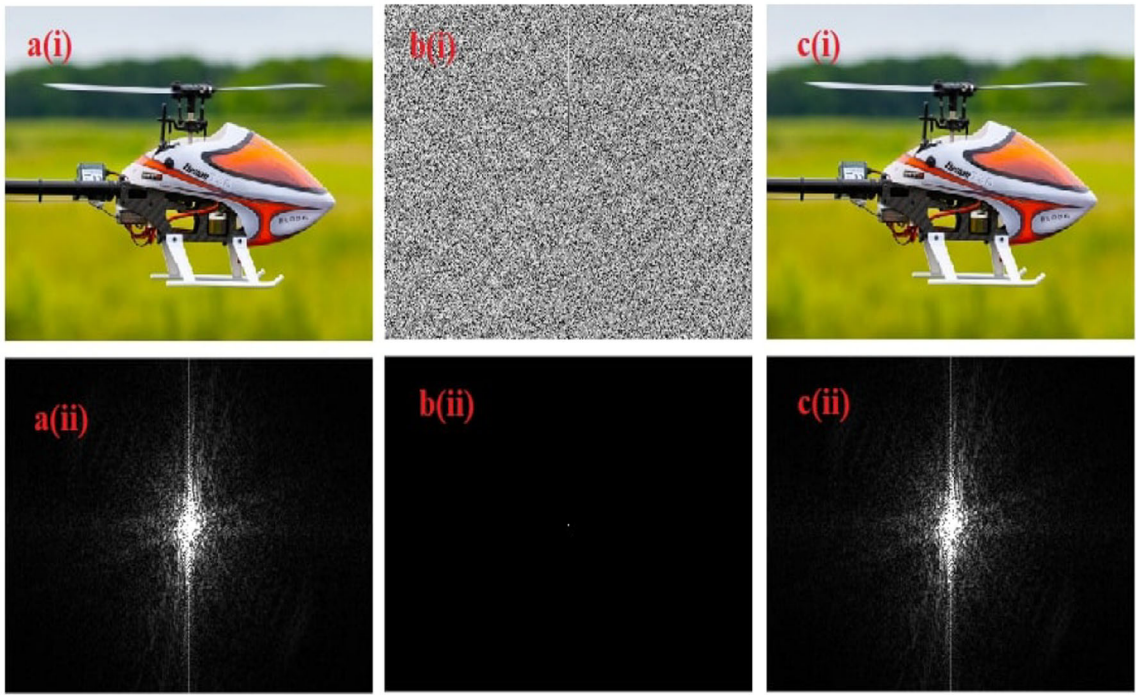

Fig. 11 Chaos communication: **a**(i) The original input image (I), **b**(i) the encrypted image (I_E), **c**(i) the decrypted image (I_D). The bottom panels shows **a**(ii), **b**(ii), and **c**(ii) are the corresponding fast Fourier transforms of the images I, I_E, I_D respectively

Algorithm:

1. **Input:** The colour image $I = M \times N$ is taken as 256-bit size. (row column colour)= **I** (size); $\mathbf{I_R}$=**I** (:,:, 1) [Red colour]; $\mathbf{I_G}$=**I** (:,:, 2) [Green colour]; $\mathbf{I_B}$=**I** (:,:, 3) [Blue colour]; **I**(size)=$row \times column$;
2. **Key:** The master: $g(y(t))$ and slave $g(z(t))$ systems with real and imaginary components such as $y_i(t)$, $z_i(t)$, where $i = 1, 2$ is considered a key to encrypt the image with various schemes.
3. **Encryption:** The image signals I_R, I_G, I_B can be masked through chaotic outputs via a bitwise mathematical XOR ($\oplus$) operation. The following strategies are considered:

$$\begin{cases} E_R(i) = I_R(i) \oplus z_1(R), \\ E_G(i) = I_G(i) \oplus z_2(R), \\ E_B(i) = I_B(i) \oplus z_1(Im). \end{cases} \tag{42}$$

   Note that it is not essential that the state variables be mixed for the green image signal. We performed this to obtain greater encryption complexity. Furthermore, the encrypted signals (E_R, E_G, *and* E_B) are performed by pseudo-functions and mixed with the three-color images to obtain the encryption image I_E with a size of $[M \times N]$.
4. **Output:** The plain image (I_R): In the decoding algorithm, the response system $g(z(t))$ is used to decrypt the image. The reverse process of applying the above process from Steps 1 to 3 is implemented for the process of getting the original image. Figure 11c(i) shows the decrypted image (I_D) and c(ii) its corresponding FFT image.

5.2 Statistical measures

The correlation between two images can be calculated using different methods, but a common approach is to use the Pearson correlation coefficient. The formula for the Pearson correlation coefficient (Cor) between two images (A) and (B) can be expressed as:

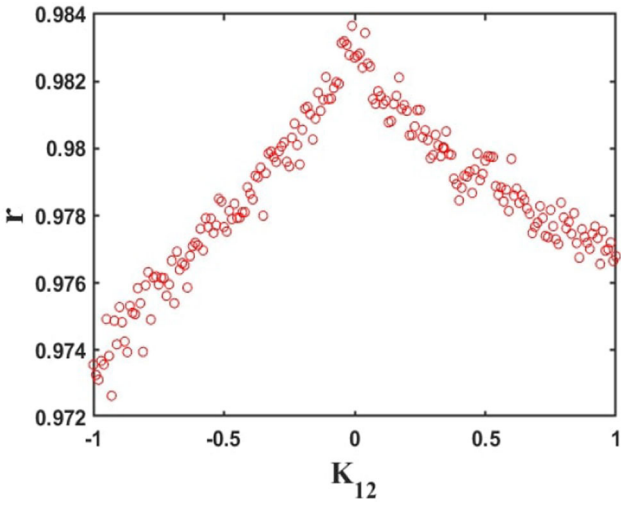

Fig. 12 Numerically computed correlation difference between original ('**A**') and decrypted ('**B**') images concerning the control gain matrix (K_1) of the Re element $K_1(1, 1)$

The correlation between the two images, i.e, original image and the output image of the communication scheme is calculated as follows:

$$\mathrm{Cor} = \frac{\sum_m \sum_n (A_{mn} - \bar{A})(B_{mn} - \bar{B})}{\sqrt{(\sum_m \sum_n (A_{mn} - \bar{A})^2)(\sum_m \sum_n (B_{mn} - \bar{B})^2)}}. \tag{43}$$

In the above Eq. (43), 'Cor' represents the correlation between the two images 'A' and 'B'. The two images are the same size as $(m \times n)$. $\bar{A}$ and $\bar{B}$ are the mean values of the images A and B that are calculated from each and every m and n. From this correlation analysis, we achieve the maximum of Cor = 0.9925 correlation coefficient values. Similarly, we tune the control gain matrix K_1 of Re element $K_1(1, 1)$ of the system. Figure 12 shows the variations in the correlation coefficients of the two images (A) and (B) of the image encryption scheme.

From this analysis, the maximum of the image correlation could occur near the positive ranges and the zero of the coupling matrix values. We took control gain matrix K_1 of Re element $K_1(1, 1)$ for tuning. Similarly, we could choose another element in the control gain matrix K_1 and K_2.

6 Conclusions

In this paper, we consider the synchronization of delayed CVNNs problem for a class of reachable set estimation with cyber-attacks and ET approach in the network environment. The event-triggered control strategy with cyberattacks is used to make implementation easier and communication more effective. It uses partial neurons instead of all ones to get the master–slave systems to work together. Combining some novel inequality techniques with the LKF method, sufficient conditions have been derived for the systems with complex values of master–slave considered. A criterion has been implemented in the set of LMIs to validate the boundedness of the reachable set of CVNNs. Testing the proposed stability criteria can be done using a standard numerical tool like the YALMIP toolbox in MATLAB. Finally, concrete examples have been used to support the validity of the theoretical findings of this work. In the proposed network, we examined successfully the novel chaotic communication using encryption and decryption mechanism and communicated an image and verified 2D fast Fourier transform. We also validated the maximum chaotic communication accuracy by varying the control element. From a thermodynamic analogy, this process can be seen as reducing the entropy of the system by stabilizing its state under constraints, effectively controlling the disorder introduced by external influences. Furthermore, the dynamics of CVNNs with Markovian jumping and impulsive effects are difficult to study, and that is what we hope to do in the future.

Acknowledgements The first author thanks Phuket Rajabhat University, Phuket, Thailand for supporting this research and the second author acknowledges the Basic Research Program of the National Research University, Higher School of Economics, Moscow.

Author contribution statement

All authors contributed equally and significantly to the writing of this article and typed, read and approved the final manuscript.

Funding Not applicable.

Data availability There is no data associated with the manuscript.

Declarations

Conflict of interest The author declares that there is no Conflict of interest regarding the publication of this paper.

Ethical approval Not applicable.

Appendix A:

$$
\begin{aligned}
\tilde{\Sigma}_{[\partial(t)]} &= \sum_{i=1}^{7}\Xi_i + \tilde{\Xi}_{11},\\
\Xi_1 &= \jmath_1\tilde{P}_\rho\jmath_{10} + \jmath_1\alpha\tilde{P}_\rho\jmath_1 + \jmath_1^*\sum_{j=1}^{N}\Pi_{\rho j}\tilde{P}_j\jmath_1\\
\Xi_2 &= \jmath_1^T(\tilde{J}_1+\tilde{J}_2)\jmath_1 - (1-\mu)e^{-\alpha\partial_1}(\jmath_2^*\tilde{J}_1\jmath_2 + \jmath_5^*\tilde{J}_3\jmath_5) - e^{-\alpha\partial_1}\jmath_3^*\tilde{J}_2\jmath_3 + \jmath_4^*\tilde{J}_3\jmath_4,\\
\Xi_3 &= \partial_1[\jmath_1\ \jmath_{10}]^*\tilde{\mathscr{G}}_1[\jmath_1\ \jmath_{10}] + \partial_1^2\jmath_{10}^*\tilde{\mathscr{G}}_2\jmath_{10} + \jmath_1^*\tilde{\mathscr{G}}_m\jmath_1 + \jmath_2^*(\tilde{\mathscr{G}}_n-\tilde{\mathscr{G}}_m)\jmath_2 + sym(\hat{J}_1\Omega_1+\hat{J}_2\Omega_2)\\
&\quad + \left(\frac{\partial_{1t}}{\partial_1}+\frac{\partial^2(t)}{\partial_1^2}\right)sym[\hat{Y}_1^*\hat{\varsigma}_1+\hat{Y}_2^*\hat{\varsigma}_2] + \jmath_3^*\tilde{\mathscr{G}}_n\jmath_3 - \left(\frac{\partial_{1t}}{\partial_1^2}\hat{\varsigma}_1^T\tilde{\mathscr{G}}_2\hat{\varsigma}_1 + \frac{\partial(t)}{\partial_1^2}\hat{\varsigma}_2^T\tilde{\mathscr{G}}_2\hat{\varsigma}_2\right),\\
\Xi_4 &= e^{-\alpha h_2}\{h_2\jmath_1^*[h_2\tilde{H}_{11}+2\tilde{H}_{13}^*]\jmath_1 + 2\jmath_1^*[h_2\tilde{H}_{12}-\tilde{H}_{13}+\tilde{H}_{23}^*]\jmath_{12}\\
&\quad + \jmath_{12}^*[h_2\tilde{H}_{22}-2\tilde{H}_{23}^*]\jmath_{12} + \jmath_{10}^*\ \{h_2^2\tilde{\mathscr{G}}_3+d_2^2\tilde{\mathscr{G}}_4\}\jmath_{10}\}\\
&\quad + e^{-\alpha d_2}\{-(\jmath_1-\jmath_{14})^*\{\mathscr{G}_4(\jmath_1-\jmath_{14}) + \mathscr{K}_1(\jmath_{14}-\jmath_{15})\} - (\jmath_{14}-\jmath_{15})^*\tilde{\mathscr{G}}_4(\jmath_{14}-\jmath_{15})\}\\
&\quad - e^{-\alpha d_2}\{\jmath_1^*\tilde{\tilde{\mathscr{G}}}_3\jmath_1 + \jmath_1^*\tilde{\tilde{\mathscr{G}}}_3\jmath_{11} - \jmath_{11}^*2\tilde{\tilde{\mathscr{G}}}_3\jmath_{11} + \jmath_{11}^*\tilde{\tilde{\mathscr{G}}}_3\jmath_{12} - \jmath_{12}^*\tilde{\tilde{\mathscr{G}}}_3\jmath_{12}\},\\
\Xi_5 &= -\jmath_1^*\hat{X}_1\tilde{\hat{\Lambda}}_1\jmath_1 + \jmath_1^*\hat{X}_2\tilde{\hat{\Lambda}}_1\jmath_4 - \jmath_4^*\tilde{\hat{\Lambda}}_1\jmath_4 - \jmath_2^*\hat{X}_1\tilde{\hat{\Lambda}}_2\jmath_2 + \jmath_2^*\hat{X}_2\tilde{\hat{\Lambda}}_2\jmath_5 - \jmath_5^*\tilde{\hat{\Lambda}}_2\jmath_5,\\
\Xi_6 &= [k_1I,\ 0,\ 0,\ k_3I,\ k_4I,\ 0,\ 0,\ 0,\ 0,\ k_2I,\ 0,\ 0,\ 0,\ 0,\ 0,\ 0,\ 0]^*\\
&\quad \times[-\bar{M}_\rho\bar{\mathbb{W}},\ 0,\ 0,\ \bar{N}_\rho\bar{\mathbb{W}},\ \bar{O}_\rho\bar{\mathbb{W}},\ 0,\ 0,\ 0,\ 0,\ -\bar{\mathbb{W}},\ \Omega_{11},\ 0,\ \Omega_{13},\ 0,\ 0,\ \Omega_{16},\ \bar{E}_\rho\bar{\mathbb{W}}],\\
\Xi_7 &= \phi\jmath_{11}^*\bar{\Theta}_\rho\jmath_{11} - \jmath_{13}^*\bar{\Theta}_\rho\jmath_{13},\\
\Omega_{11} &= \bar{\beta}(2-\bar{\beta})\mathbb{Y}_\rho,\ \ \Omega_{13} = \bar{\beta}(2-\bar{\beta})\mathbb{Y}_\rho,\\
\Omega_{16} &= (1-\bar{\beta})^2\mathbb{Y}_\rho,\ \ \tilde{\Xi}_{11} = \jmath_{19}^*\frac{-\alpha}{\hat{w}^2}I\jmath_{19},\\
\tilde{\Psi}_{12} &= \sqrt{\partial_1}\hat{J}_2^*,\ \ \tilde{\Psi}_{13} = \sqrt{\partial_1}\hat{Y}_2^*,\\
\tilde{\Psi}_{22} &= -e^{2\alpha\partial_1}\tilde{\mathscr{G}}_n,\ \ \tilde{\Psi}_{33} = -e^{\alpha\partial_1}\tilde{\mathscr{G}}_2,\ \ \bar{\Psi}_{12} = \sqrt{\partial_1}\hat{J}_1^*,\\
\bar{\Psi}_{13} &= \sqrt{\partial_1}\hat{Y}_1^*,\ \ \bar{\Psi}_{22} = -e^{2\alpha\partial_1}\tilde{\mathscr{G}}_m,\ \ \bar{\Psi}_{33} = -e^{\alpha\partial_1}\tilde{\mathscr{G}}_2.
\end{aligned}
$$

References

1. C. Lee, H. Hasegawa, S. Gao, Complex-valued neural networks: a comprehensive survey. IEEE/CAA J. Automat. Sinica **9**(8), 1406–1426 (2022)
2. S. Chen, L. Hanzo, S. Tan, Symmetric complex-valued RBF receiver for multiple-antenna-aided wireless systems. IEEE Trans. Neural Netw. **19**(9), 1659–1665 (2008)

3. S. Cuomo, V.S. Di Cola, F. Giampaolo, G. Rozza, M. Raissi, F. Piccialli, Scientific machine learning through physics-informed neural networks: where we are and what's next. J. Sci. Comput. **92**(3), 88 (2022)
4. S. Cai, Z. Mao, Z. Wang, M. Yin, G.E. Karniadakis, Physics-informed neural networks (pinns) for fluid mechanics: a review. Acta Mech. Sinica **37**(12), 1727–1738 (2021)
5. J.W. Woolley, P. Agarwal, J. Baker, Modeling and prediction of chaotic systems with artificial neural networks. Int. J. Numer. Methods Fluids **63**(8), 989–1004 (2010)
6. Jd.J. Serrano-Pérez, G. Fernández-Anaya, S. Carrillo-Moreno, W. Yu, New results for prediction of chaotic systems using deep recurrent neural networks. Neural Process. Lett **53**, 1579–1596 (2021)
7. B. Hkdh, Neural networks in materials science. ISIJ Int. **39**(10), 966–979 (1999)
8. A. Hirose, Complex-valued neural networks. IEEJ Trans. Electron. Inform. Syst. **131**(1), 2–8 (2011)
9. S. Gupta, R. Zia, Quantum neural networks. J. Comput. Syst. Sci. **63**(3), 355–383 (2001)
10. Y. Zhang, H. Huang, Adaptive complex-valued stepsize-based fast learning of complex-valued neural networks. Neural Netw. **124**, 233–242 (2020)
11. G. Chen, Z. Pei, H. Yang, Y. Ma, B. Yu, M. Wong, Physics-informed optical kernel regression using complex-valued neural fields. In: 2023 60th ACM/IEEE Design Automation Conference (DAC), pp. 1–6 (2023). IEEE
12. R. Savitha, S. Suresh, N. Sundararajan, A fully complex-valued radial basis function network and its learning algorithm. Int. J. Neural Syst. **19**(04), 253–267 (2009)
13. R. Wu, H. Huang, X. Qian, T. Huang, A L-BFGS based learning algorithm for complex-valued feedforward neural networks. Neural Process. Lett. **47**, 1271–1284 (2018)
14. J. Pan, X. Liu, W. Xie, Exponential stability of a class of complex-valued neural networks with time-varying delays. Neurocomputing **164**, 293–299 (2015)
15. J. Jian, P. Wan, Global exponential convergence of fuzzy complex-valued neural networks with time-varying delays and impulsive effects. Fuzzy Sets Syst. **338**, 23–39 (2018)
16. R. Guo, W. Lv, Z. Zhang, Quasi-projective synchronization of stochastic complex-valued neural networks with time-varying delay and mismatched parameters. Neurocomputing **415**, 184–192 (2020)
17. Q. Song, Z. Zhao, Stability criterion of complex-valued neural networks with both leakage delay and time-varying delays on time scales. Neurocomputing **171**, 179–184 (2016)
18. M.S. Ali, R. Vadivel, R. Saravanakumar, Event-triggered state estimation for Markovian jumping impulsive neural networks with interval time-varying delays. Int. J. Control **92**(2), 270–290 (2019)
19. R. Vadivel, M.S. Ali, F. Alzahrani, Robust H_∞ synchronization of Markov jump stochastic uncertain neural networks with decentralized event-triggered mechanism. Chin. J. Phys. **60**, 68–87 (2019)
20. X. Song, J. Man, C.K. Ahn, S. Song, Synchronization in finite/fixed time for Markovian complex-valued nonlinear interconnected neural networks with reaction-diffusion terms. IEEE Trans. Netw. Sci. Eng. **8**(4), 3313–3324 (2021)
21. R.V. Aravind, P. Balasubramaniam, Stochastic stability of fractional-order Markovian jumping complex-valued neural networks with time-varying delays. Neurocomputing **439**, 122–133 (2021)
22. X. Song, J. Man, S. Song, Y. Zhang, Z. Ning, Finite/fixed-time synchronization for Markovian complex-valued memristive neural networks with reaction-diffusion terms and its application. Neurocomputing **414**, 131–142 (2020)
23. X. Xu, Q. Xu, Y. Peng, J. Zhang, Y. Xu, Stochastic exponential robust stability of delayed complex-valued neural networks with Markovain jumping parameters. IEEE Access **6**, 839–849 (2017)
24. M. Hui, N. Yao, H.H.-C. Iu, R. Yao, L. Bai, Adaptive synchronization of fractional-order complex-valued neural networks with time-varying delays. IEEE Access **10**, 45677–45688 (2022)
25. A. Kumar, S. Das, V.K. Yadav et al., Global quasi-synchronization of complex-valued recurrent neural networks with time-varying delay and interaction terms. Chaos Soliton. Fract. **152**, 111323 (2021)
26. X. Li, W. Zhang, J.-A. Fang, H. Li, Event-triggered exponential synchronization for complex-valued memristive neural networks with time-varying delays. IEEE Trans. Neural Netw. Learn. Syst. **31**(10), 4104–4116 (2019)
27. Y. Shen, X. Liu, Event-based master-slave synchronization of complex-valued neural networks via pinning impulsive control. Neural Netw. **145**, 374–385 (2022)
28. L.M. Pecora, T.L. Carroll, Synchronization in chaotic systems. Phys. Rev. Lett. **64**(8), 821 (1990)
29. Y. Yuan, Q. Song, Y. Liu, F.E. Alsaadi, Synchronization of complex-valued neural networks with mixed two additive time-varying delays. Neurocomputing **332**, 149–158 (2019)
30. X. Li, J.-A. Fang, H. Li, Master-slave exponential synchronization of delayed complex-valued memristor-based neural networks via impulsive control. Neural Netw. **93**, 165–175 (2017)
31. N. Gunasekaran, G. Zhai, Stability analysis for uncertain switched delayed complex-valued neural networks. Neurocomputing **367**, 198–206 (2019)
32. N. Gunasekaran, G. Zhai, Sampled-data state-estimation of delayed complex-valued neural networks. Int. J. Syst. Sci. **51**(2), 303–312 (2020)
33. R. Vadivel, P. Hammachukiattikul, Q. Zhu, N. Gunasekaran, Event-triggered synchronization for stochastic delayed neural networks: passivity and passification case. Asian J. Control **25**(4), 2681–2698 (2023)
34. W. Xiang, H.-D. Tran, X. Yang, T.T. Johnson, Reachable set estimation for neural network control systems: a simulation-guided approach. IEEE Trans. Neural Netw. Learn. Syst. **32**(5), 1821–1830 (2020)
35. V. Rajarathinam, Event-triggered stabilization of delayed complex-valued neural networks via reachable set estimation. In: 2022 37th International Technical Conference on Circuits/Systems, Computers and Communications (ITC-CSCC), pp. 567–570. IEEE (2022)

36. Y. Gao, S. Zhu, J. Li, Reachable set bounding for a class of memristive complex-valued neural networks with disturbances. Neurocomputing **385**, 368–377 (2020)
37. S. Zhu, Y. Gao, Y. Hou, C. Yang, Reachable set estimation for memristive complex-valued neural networks with disturbances. IEEE Trans. Neural Netw. Learn. Syst. (2022)
38. R. Vadivel, P. Hammachukiattikul, N. Gunasekaran, R. Saravanakumar, H. Dutta, Strict dissipativity synchronization for delayed static neural networks: an event-triggered scheme. Chaos Solitons Fract. **150**, 111212 (2021)
39. S. Senan, M.S. Ali, R. Vadivel, S. Arik, Decentralized event-triggered synchronization of uncertain Markovian jumping neutral-type neural networks with mixed delays. Neural Netw. **86**, 32–41 (2017)
40. Y. Wang, S. Ding, R. Li, Master-slave synchronization of neural networks via event-triggered dynamic controller. Neurocomputing **419**, 215–223 (2021)
41. J. Liu, Y. Wang, J. Cao, D. Yue, X. Xie, Secure adaptive-event-triggered filter design with input constraint and hybrid cyber attack. IEEE Trans. Cybern. **51**(8), 4000–4010 (2020)
42. J. Liu, W. Suo, X. Xie, D. Yue, J. Cao, Quantized control for a class of neural networks with adaptive event-triggered scheme and complex cyber-attacks. Int. J. Robust Nonlinear Control **31**(10), 4705–4728 (2021)
43. R. Pan, Y. Tan, D. Du, S. Fei, Adaptive event-triggered synchronization control for complex networks with quantization and cyber-attacks. Neurocomputing **382**, 249–258 (2020)
44. M. Li, J. Zhao, J. Xia, G. Zhuang, W. Zhang, Extended dissipative analysis and synthesis for network control systems with an event-triggered scheme. Neurocomputing **312**, 34–40 (2018)
45. W.-J. Lin, Y. He, M. Wu, Q. Liu, Reachable set estimation for Markovian jump neural networks with time-varying delay. Neural Netw. **108**, 527–532 (2018)
46. L. Zha, E. Tian, X. Xie, Z. Gu, J. Cao, Decentralized event-triggered H_∞ control for neural networks subject to cyber-attacks. Inform. Sci. **457**, 141–155 (2018)
47. Y. Tian, Z. Wang, Composite slack-matrix-based integral inequality and its application to stability analysis of time-delay systems. Appl. Math. Lett. **120**, 107252 (2021)
48. Y. Liu, J.H. Park, F. Fang, Global exponential stability of delayed neural networks based on a new integral inequality. IEEE Trans. Syst. Man Cybern. Syst. **49**(11), 2318–2325 (2018)
49. P.-L. Liu, Improved delay-dependent robust stability criteria for recurrent neural networks with time-varying delays. ISA Trans. **52**(1), 30–35 (2013)
50. S. Kim, P. Park, C. Jeong, Robust H_∞ stabilisation of networked control systems with packet analyser. IET Control Theory Appl. **4**(9), 1828–1837 (2010)
51. M.S. Ali, N. Gunasekaran, R. Saravanakumar, Design of passivity and passification for delayed neural networks with Markovian jump parameters via non-uniform sampled-data control. Neural Comput. Appl. **30**(2), 595–605 (2018)